



HAL
open science

Structural determinants of bacterial lytic polysaccharide monooxygenase functionality

Zarah Forsberg, Bastien Bissaro, Jonathan Gullesen, Bjørn Dalhus, Gustav Vaaje-Kolstad, Vincent G. H. Eijsink

► To cite this version:

Zarah Forsberg, Bastien Bissaro, Jonathan Gullesen, Bjørn Dalhus, Gustav Vaaje-Kolstad, et al.. Structural determinants of bacterial lytic polysaccharide monooxygenase functionality. *Journal of Biological Chemistry*, 2018, 293 (4), pp.1397-1412. 10.1074/jbc.M117.817130 . hal-01886474

HAL Id: hal-01886474

<https://hal.science/hal-01886474>

Submitted on 26 May 2020

HAL is a multi-disciplinary open access archive for the deposit and dissemination of scientific research documents, whether they are published or not. The documents may come from teaching and research institutions in France or abroad, or from public or private research centers.

L'archive ouverte pluridisciplinaire **HAL**, est destinée au dépôt et à la diffusion de documents scientifiques de niveau recherche, publiés ou non, émanant des établissements d'enseignement et de recherche français ou étrangers, des laboratoires publics ou privés.

Copyright



Structural determinants of bacterial lytic polysaccharide monoxygenase functionality

Received for publication, September 11, 2017, and in revised form, November 22, 2017 Published, Papers in Press, December 8, 2017, DOI 10.1074/jbc.M117.817130

Zarah Forsberg^{†1}, Bastien Bissaro^{‡§}, Jonathan Gullesen[‡], Bjørn Dalhus^{¶||}, Gustav Vaaje-Kolstad[‡], and Vincent G. H. Eijsink[‡]

From the [†]Faculty of Chemistry, Biotechnology, and Food Science, Norwegian University of Life Sciences (NMBU), 1432 Ås, Norway, [§]INRA, UMR792, Ingénierie des Systèmes Biologiques et des Procédés, F-31400 Toulouse, France, and the [¶]Department of Medical Biochemistry, Institute for Clinical Medicine, University of Oslo, 0318 Oslo, Norway, and the ^{||}Department of Microbiology, Clinic for Laboratory Medicine, Oslo University Hospital, Rikshospitalet, P. O. Box 4950, Nydalen, N-0424 Oslo, Norway

Edited by Ruma Banerjee

Bacterial lytic polysaccharide monoxygenases (LPMO10s) use redox chemistry to cleave glycosidic bonds in the two foremost recalcitrant polysaccharides found in nature, namely cellulose and chitin. Analysis of correlated mutations revealed that the substrate-binding and copper-containing surface of LPMO10s composes a network of co-evolved residues and interactions, whose roles in LPMO functionality are unclear. Here, we mutated a subset of these correlated residues in a newly characterized C1/C4-oxidizing LPMO10 from *Micromonospora aurantiaca* (*Ma*LPMO10B) to the corresponding residues in strictly C1-oxidizing LPMO10s. We found that surface properties near the catalytic copper, *i.e.* side chains likely to be involved in substrate positioning, are major determinants of the C1:C4 ratio. Several *Ma*LPMO10B mutants almost completely lost C4-oxidizing activity while maintaining C1-oxidizing activity. These mutants also lost chitin-oxidizing activity, which is typically observed for C1/C4-oxidizing, but not for C1-oxidizing, cellulose-active LPMO10s. Selective loss in C1-oxidizing activity was not observed. Additional mutational experiments disclosed that neither truncation of the *Ma*LPMO10B family 2 carbohydrate-binding module nor mutations altering access to the solvent-exposed axial copper coordination site significantly change the C1:C4 ratio. Importantly, several of the mutations that altered interactions with the substrate exhibited reduced stability. This effect could be explained by productive substrate binding that protects LPMOs from oxidative self-inactivation. We discuss these stability issues in view of recent findings on LPMO catalysis, such as the involvement of H₂O₂. Our results

show that residues on the substrate-binding surface of LPMOs have co-evolved to optimize several of the interconnected properties: substrate binding and specificity, oxidative regioselectivity, catalytic efficiency, and stability.

Microorganisms that utilize structural carbohydrates, such as cellulose and chitin, as a source of energy secrete a plethora of hydrolytic and oxidative enzymes. Among these are the recently discovered copper-dependent lytic polysaccharide monoxygenases (LPMOs)² (1–3), which use oxidative chemistry to cleave polysaccharides. By carrying out cleavages in crystalline regions of polysaccharides, LPMOs make the substrate more tractable to the action of canonical endo- and exo-cellulases (1, 4, 5). Today, it is widely recognized that LPMO-catalyzed oxidative processes play a major role in microbial conversion of recalcitrant polysaccharides through a synergistic interplay with hydrolytic (6, 7) as well as other redox-active enzymes (3, 8–11). The catalytic mechanism of LPMOs remains poorly understood (12–15). The reaction is generally considered to require molecular oxygen and two externally delivered electrons (1). Recently, an alternative mechanism involving H₂O₂ rather than O₂ has been proposed (16).

As of 2013, LPMOs have been classified into four of the 13 families of auxiliary activities (AA9–11 and 13) in the database for carbohydrate-active enzymes (CAZy) (17). Members of families AA9, -11, and -13 are of fungal origin, whereas the bacterial LPMOs group in family AA10. AA9 LPMOs (LPMO9s) are known to act on cellulose (2, 18, 19), cello-oligosaccharides (20), xyloglucan, glucomannan (21), and xylan (22). In terms of the oxidative regioselectivity, three types of cellulose-oxidizing LPMO9s have been described, namely those that strictly oxidize the C1- or the C4-carbon and those that can oxidize both (Fig. 1) (23). For AA10 LPMOs (LPMO10s), activity toward

This work was supported by Research Council of Norway Grants 214138, 214613, and 226247 (to G. V.-K. and V. G. H. E.), by Vista Programme of the Norwegian Academy of Science and Letters Grant 6510 (to Z. F.), by European Union in the framework of the Marie-Curie FP7 COFUND People Programme (through the award of an AgreenSkills Fellowship under Grant 267196), by the French Institut National de la Recherche Agronomique (INRA) (to B. B.), and by the South-Eastern Norway Regional Health Authority Grant 2015095 (Regional Core Facility for Structural Biology) (to B. D.). The authors declare that they have no conflicts of interest with the contents of this article.

This article contains Figs. S1–S14, Tables S1–S8 and supporting Refs. 1–7. The atomic coordinates and structure factors (code 5OPF) have been deposited in the Protein Data Bank (<http://www.pdb.org/>).

¹ To whom correspondence should be addressed: Faculty of Chemistry, Biotechnology, and Food Science, The Norwegian University of Life Sciences (NMBU), 1432 Ås, Norway. Tel.: 47-67232469; E-mail: zarah.forsberg@nmbu.no.

² The abbreviations used are: LPMO, lytic polysaccharide monoxygenase; GlcGlc1A, aldonic acid of cellobiose; AA, auxiliary activity; CBM, carbohydrate-binding module; CMA, correlated mutation analysis; Glc4GemGlc, gemdiol of cellobiose; MtCDH, *Mycobacterium thermophilum* cellobiose dehydrogenase; MSA, multiple sequence alignment; PASC, phosphoric acid swollen cellulose; PDB, Protein Data Bank; BisTris, 2-[bis(2-hydroxyethyl)amino]-2-(hydroxymethyl)propane-1,3-diol; Bistrispropane, 1,3-bis[tris(hydroxymethyl)methylamino]propane; cd, catalytic domain; HPAEC-PAD, high-performance anion-exchange chromatography with pulsed amperometric detection.

Functionality of cellulose-oxidizing LPMO10s

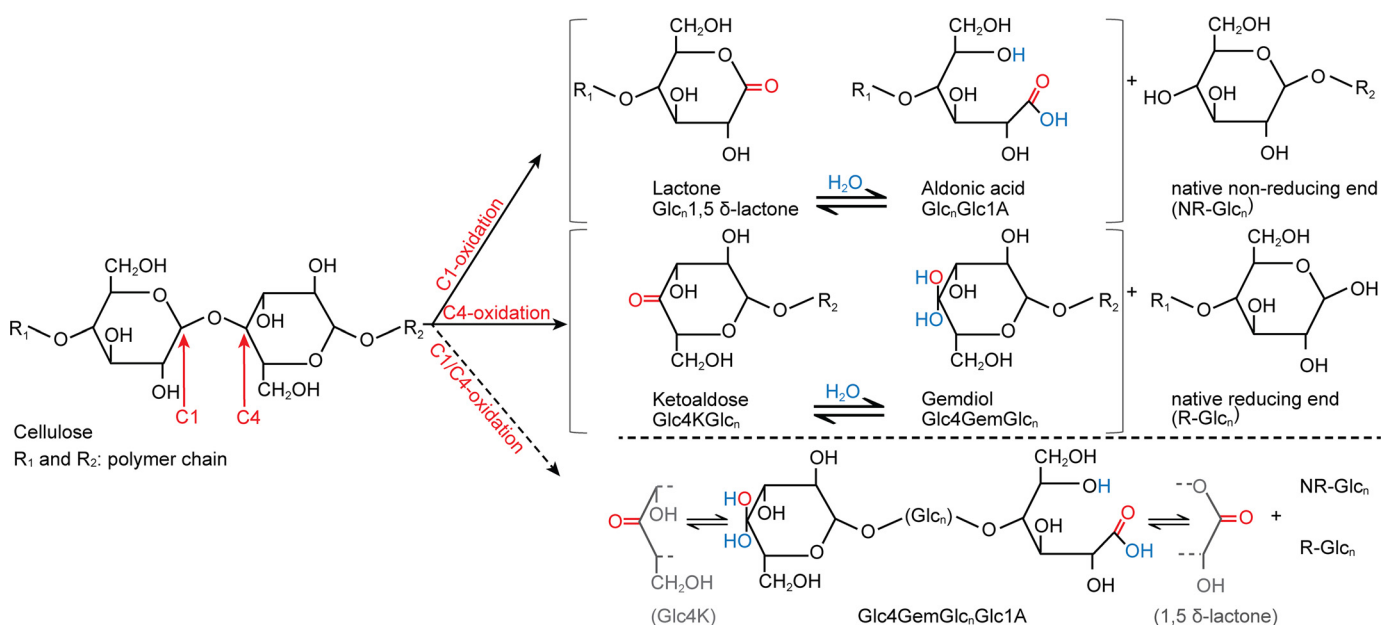


Figure 1. Oxidative regioselectivity in cellulose-active LPMOs. C1 oxidation (*upper scheme*) results in the formation of lactones that are hydrated to aldonic acids and generate native non-reducing ends. C4 oxidation (*middle scheme*) leads to the formation of ketoaldoses and the corresponding hydrated gemdiols and generates native reducing ends. LPMOs with mixed C1/C4 oxidation can, in addition to the abovementioned compounds, also produce oligosaccharides that are oxidized at both ends (*i.e.* C1/C4 double-oxidized products).

chitin (1) and cellulose (24) or both (25) has been described. All hitherto characterized chitin-active LPMO10s oxidize exclusively the C1-carbon atom, whereas those that act on cellulosic substrates have been shown to either exclusively oxidize the C1 position or generate a mixture of C1- and C4-oxidized products (25). Furthermore, LPMO10s that can oxidize both the C1- and the C4-carbon in cellulose are also capable of oxidizing the C1-carbon in chitin (25). C1 oxidation results in the formation of 1,5- δ -lactones, which are spontaneously converted to the hydrated and more stable aldonic acid forms (Glc_nGlc1A) at neutral pH (26). LPMOs that oxidize the non-reducing end (C4-oxidizers) produce 4-ketoaldoses (Glc4KGlc_n) that are spontaneously hydrated to their corresponding gemdiol (Glc4GemGlc_n) form (Fig. 1) (20). LPMOs with mixed C1/C4 activity can generate double-oxidized products (25), which result from two oxidative cleavages in the same polymer chain.

Although members of different LPMO families share low sequence identity, their structural resemblance is conspicuous. The pyramidal core structure of LPMOs consists of a distorted β -sandwich comprising two β -sheets that are connected by a varying number of loops and helices. The surface-exposed active site is part of a flat substrate-binding surface (2, 27, 28) and comprises a copper ion coordinated by two histidines in a T-shaped geometry. Because this copper site is conserved in all types of LPMOs, variation in enzyme performance, substrate specificity, and oxidative regioselectivity must be driven by variation in surrounding amino acids that constitute the binding surface. In LPMO10s, the substrate-binding surface is made up of 20–30 amino acids covering an area of ~ 30 by 40 Å (29). Despite increasing knowledge on how LPMOs interact with their substrate (27, 28, 30), still little is known about the structural determinants of substrate specificity and oxidative regioselectivity.

Structural comparisons have revealed a correlation between the accessibility of the solvent-exposed axial copper-coordination site and oxidative regioselectivity (25, 31) that awaits experimental verification. Experimental data on oxidative regioselectivity from Vu *et al.* (23) showed that removal of an extra loop, which is found in LPMO9s that can oxidize both C1 and C4 in cellulose, eliminated the ability to oxidize the C4-carbon, whereas the C1 activity was preserved. This finding correlates well with the fact that this loop is lacking in LPMO9s that exclusively oxidize C1, but it is more intriguing when considering that strictly C4-oxidizing LPMO9s also lack this loop. It seems that other determinants for oxidative regioselectivity are still to be discovered. On this note, Danneels *et al.* (32) recently showed that aromatic residues on the surface of LPMO9s affect oxidative regioselectivity.

In this study, we have compared sequences of LPMO10s that oxidize cellulose at either the C1 or at the C1- and C4-carbons. Surface-exposed residues identified by correlated mutation analysis (33) as well as residues affecting the accessibility of the solvent-exposed axial copper-coordination site were targeted by site-directed mutagenesis. As part of these studies aimed at identifying structural determinants of LPMO functionality and focusing on oxidative regioselectivity, a previously uncharacterized LPMO10 from the bacterium *Micromonospora aurantiaca* (MaLPMO10B), with predicted mixed C1/C4 activity, was structurally and functionally characterized, including an assessment of the role of its family 2 carbohydrate-binding module (CBM2). Apart from unraveling determinants of oxidative regioselectivity, these site-directed mutagenesis studies provide some insight into the structural determinants of substrate specificity. This study also reveals mutational effects on enzyme stability that are likely related to changes in the rate of production and consumption of H₂O₂.

Results

Sequence diversity analysis and identification of putative structural determinants of LPMO functionality

Facing the scarcity of regioselectivity-related mutagenesis data, we set out to harness information given by natural sequence diversity, focusing on co-evolved residues that could be involved in the divergence between C1-specific and C1/C4-oxidizing cellulose-active LPMO10s. A sequence analysis was carried out with 54 sequences (Table S1) putatively encoding for the C1-specific and the C1/C4-oxidizing cellulose-active LPMO10s (Fig. 2). The global analysis pipeline consisted of the following steps: 1) retrieving the sequences from a larger phylogenetic analysis performed in-house that included all substrate specificities within the AA10 family (*i.e.* chitin and cellulose; see Fig. S1); 2) performing a structure-guided multiple sequence alignment (MSA); 3) carrying out a correlated mutation analysis (CMA (33)) to produce a heat map of correlated mutations (Fig. S2) and to build a correlation network (Fig. 3A); 4) mapping the correlated residues on the 3D structure (Fig. 3, B and C); and 5) selecting residues for mutational analysis based on CMA results, their spatial location relative to the active site, and existing mutagenesis data. The phylogenetic tree generated in step 1 (Fig. S1) shows two distinct subgroups corresponding to C1-specific and C1/C4-oxidizing cellulose-active LPMO10s. ScLPMO10C (also known as CelS2) and ScLPMO10B are well-studied (25) representatives of each subgroup and were defined as reference sequences for the calculation of sequence identities (Fig. 2).

Although the CMA was carried out independently of any phenotypic and structural information, the resulting networks of correlated mutations (with a correlation cutoff = 0.9) contained amino acids that differ between the two phenotypic subgroups (Fig. 3A), while being highly conserved within each subgroup (Figs. S3 and S4). Mapping the identified correlated residues on the structure of the model enzymes ScLPMO10B and ScLPMO10C showed that the correlated residues cluster at or near the substrate-binding surface and near the copper site (Fig. 3, B and C). On the basis of the structural mapping, the 13 residues were divided into three clusters (Fig. 3). The first cluster includes Pro-145 and Gly-146 on one loop and Arg-212, Asp-214, Glu-217, and Phe-219 on another interacting loop (ScLPMO10C numbering). With the exception of Phe-219, these residues are located at the surface and generally show high correlation factors (>0.97 for several couples). The second cluster (Leu-47, Asp-51, Gly-57, and Asn-63) includes residues that are relatively distant from the active site and the substrate-binding surface. The third cluster includes Tyr-79, Phe-82, and Phe-113 and shows lower correlation factors, except for the Phe-82–Phe-113 pair, for which the correlation factor is 1.00 (see Tables S2–S6 for details on the correlations within this cluster). Trp-141 was not initially identified by the CMA because three kinds of residues are found in the sequence diversity at this position (Trp, Gln, or Gly), which increases the number of potential pairs with other positions and thus decreases the correlation factor. Nevertheless, for reasons explained below, Trp was added to this third cluster. Structural superposition showed that residues in the third cluster aligned better

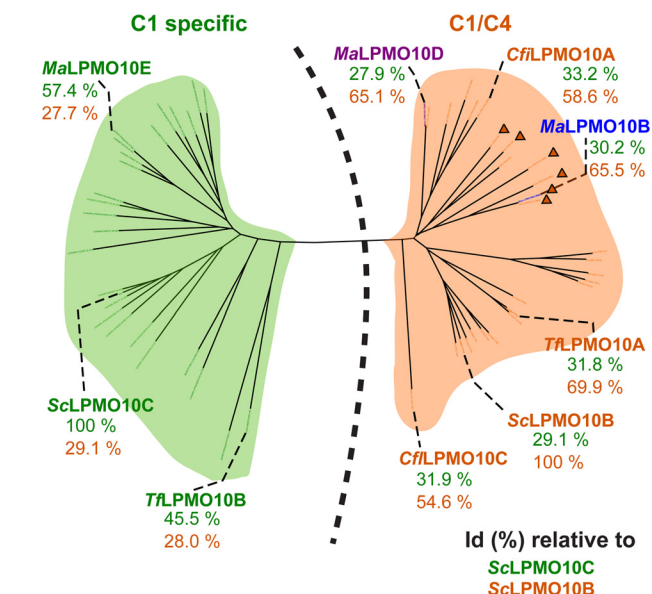


Figure 2. Phylogenetic tree of cellulose-oxidizing LPMO10s. The tree was constructed via PhyML using an MSA of the sequences of 26 predicted C1-specific and 28 predicted C1/C4-oxidizing LPMO10s as input. The sequence identities relative to ScLPMO10C (green) or ScLPMO10B (orange) are provided in the figure and are based on comparison of LPMO domains only (*e.g.* excluding signal peptides, potential linkers, and CBMs). LPMOs from *Streptomyces coelicolor*, *Thermobifida fusca*, and *Cellulomonas fimi* have been experimentally characterized (25, 34), and their names appear in the figure. The names of the three *MaLPMO10s* with predicted cellulose activity and (uncharacterized) *CflLPMO10C*, which was used as a sequence boundary for the C1/C4 group, also appear in the figure. Orange triangles indicate sequences that contain an insertion that also occurs in *MaLPMO10B* as discussed in the main text. The sequences of the LPMOs shown in this picture are provided in Table S1.

than residues in the first cluster. Because of this and because residues equivalent to Tyr-79, Phe-82, and Trp-141 had previously been shown to be involved in substrate recognition by a chitin-active LPMO10 (27, 35), the third cluster (gray in Fig. 3) was selected for further studies.

Two novel LPMOs: *M. aurantiaca* LPMO10B and LPMO10D

A new model enzyme was selected as a starting platform for carrying out structure–function studies, namely the LPMO10B from *M. aurantiaca* (*MaLPMO10B*). In contrast to ScLPMO10B, *MaLPMO10B* carries a CBM (CBM2) and both published work and unpublished data from our laboratory have shown that CBMs render the LPMO more active and stable (25, 34, 36). According to the CAZy database, the *M. aurantiaca* genome encodes five LPMO10s with different putative activities. *MaLPMO10B* and *MaLPMO10D* cluster within the subgroup of C1/C4 cellulose-active LPMO10s; *MaLPMO10E* clusters with C1-specific cellulose-active LPMO10s (Fig. 2); *MaLPMO10C* clusters with chitin-active LPMO10s; and *MaLPMO10A* is a cell wall-anchored enzyme of unknown activity (see Fig. S1). In this study, the putatively C1/C4-oxidizing *MaLPMO10D*, containing a CBM2, was also expressed. The nature of correlated residues is almost identical for *MaLPMO10B*, *MaLPMO10D*, and ScLPMO10B (Fig. 3).

MaLPMO10B and *MaLPMO10D* were recombinantly expressed, and the activity was tested on cellulose and chitin substrates, including ScLPMO10B (a known C1/C4-oxidizer (25)), ScLPMO10C (a known cellulose C1-oxidizer (25)), and

Functionality of cellulose-oxidizing LPMO10s

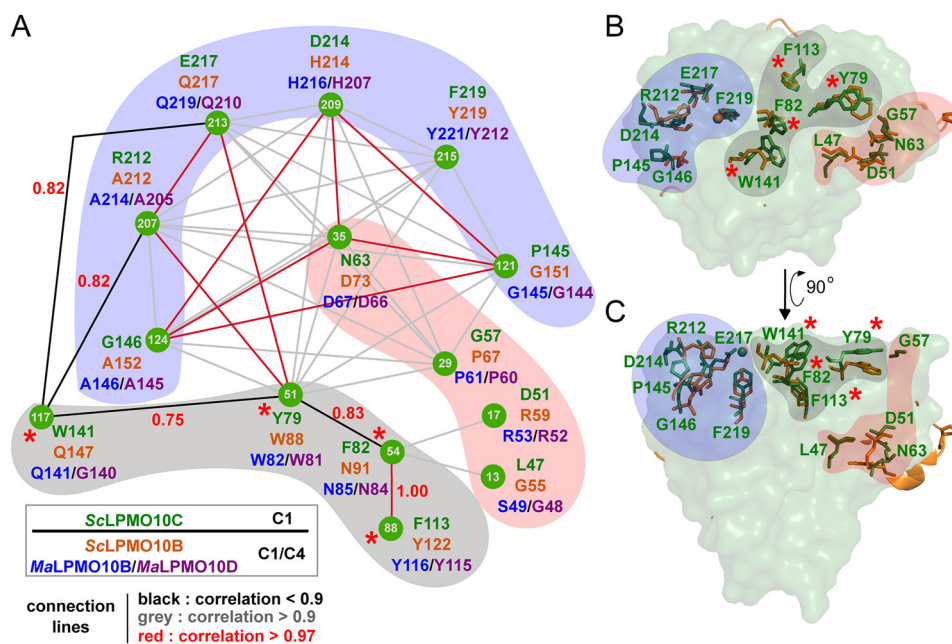


Figure 3. CMA of cellulose-oxidizing LPMO10s belonging to the C1- and C1/C4-oxidizer groups. A shows networks of correlated mutations; numbers in green circles represent the position of the residues in the MSA, and below each number the amino acids found at this position in C1-oxidizing ScLPMO10C (green), and C1/C4-oxidizing ScLPMO10B (orange), MaLPMO10B (blue), or MaLPMO10D (purple) are provided. Solid lines connecting two positions represent a correlation, with a correlation factor above 0.9 (gray) or 0.97 (red). As is common in CMA (33), existing mutagenesis data and, in particular, structural analyses were used to identify other potentially relevant connections, involving positions 51, 54, 117, 207, and 213 (black lines). B and C (top and side view, respectively) show mapping of the selected residues onto the superposed structures of ScLPMO10C (PDB 4OY7, side chains colored green) and ScLPMO10B (PDB 4OY6, side chains colored orange), which led to the designation of the three spatially separated clusters (blue, gray, and red) that are also indicated in A. The numbering provided in B and C is that of ScLPMO10C. Positions that were targeted by site-directed mutagenesis are highlighted by a red star. The copper ions are indicated by orange (ScLPMO10B) or green (ScLPMO10C) spheres.

the *Serratia marcescens* LPMO (*SmLPMO10A*, a known chitin C1-oxidizer (1)) for comparison. In agreement with the phylogeny-based prediction, analysis by HPAEC-PAD and MALDI-TOF MS of products generated from PASC degradation revealed that both *M. aurantiaca* LPMOs produce a mixture of C1-, C4-, and double-oxidized (C1/C4) cello-oligosaccharides (Fig. 4A and Fig. S5). LPMOs with a covalently attached CBM2 (ScLPMO10C, MaLPMO10B, and MaLPMO10D) generated more products than ScLPMO10B, which does not have a CBM. The product profiles showed that MaLPMO10B produced more C4-oxidized products than the two other C1/C4-oxidizing LPMO10s (MaLPMO10D and ScLPMO10B), whereas ScLPMO10C, as expected, generated C1-oxidized species only (Fig. 4A). As observed previously for ScLPMO10B (25), and in contrast to the C1-oxidizing ScLPMO10C, the two novel C1/C4-oxidizers were also active on chitin (Fig. 4B and Fig. S6). Interestingly, in contrast to chitin-specific *SmLPMO10A* (also known as CBP21 (1)), the three LPMOs with dual-substrate specificity generated considerable amounts of partially deacetylated chito-oligosaccharides (see MALDI-TOF MS Fig. S6).

Crystal structure of the catalytic domain of MaLPMO10B

The structure of the catalytic domain (cd) of MaLPMO10B (residues 37–230, lacking the linker and the CBM2), called MaLPMO10B^{cd}, was determined to 1.08 Å with a single molecule in the asymmetric unit (Table 1). The structure shows the typical LPMO fold with a central β -sandwich made up by two distorted β -sheets connected by several loops and helices (Fig. 5A). The first β -sheet is formed by three antiparallel β -strands

(S1, S4, and S8), and the second β -sheet is built up by four antiparallel strands (S5, S6, S9, and S10). Two small β -strands are located antiparallel (S2) or parallel (S3) to S10 in the four-stranded sheet. Another small β -strand (S7) is located in an insertion and lies antiparallel relative to S8. This insertion, which includes 11 residues (Pro-180–Gly-190) and extends the substrate-binding surface in MaLPMO10B (Fig. 5), occurs in only six out of the 28 C1/C4-oxidizer sequences used in the CMA (Fig. 2, orange triangles). An insertion of similar length occurs in C1-oxidizing ScLPMO10C having a different conformation and sequence (Fig. S7). Notably, this insertion occurs in an otherwise rather conserved region. Most of the sequence diversity in LPMOs is found in the region between strands S1 and S3 (36–38), also known as loop 2 (abbreviated as L2 (39)). The L2 region, which consists of 74 residues in MaLPMO10B, contains seven helices of varying sizes and makes up approximately half of the substrate-binding surface (Fig. 5B). Three of the four residues that were the primary mutagenesis targets in this study (Trp-82, Asn-85, and Tyr-116) are located in the L2 region. Apart from the extra insertion (Pro-180–Gly-190) discussed above, the surfaces of MaLPMO10B and ScLPMO10B are highly similar (Fig. 5B).

The active site in MaLPMO10B is formed by His-37 and His-144 that coordinate the copper atom in a T-shaped geometry. No water molecules were found adjacent to the copper, which indicates that the copper had been reduced during data collection (29, 42). Interestingly, the conformation of Ala-142 in MaLPMO10B is consistent with the position of the active-site alanine in the two other available structures of C1/C4-oxi-

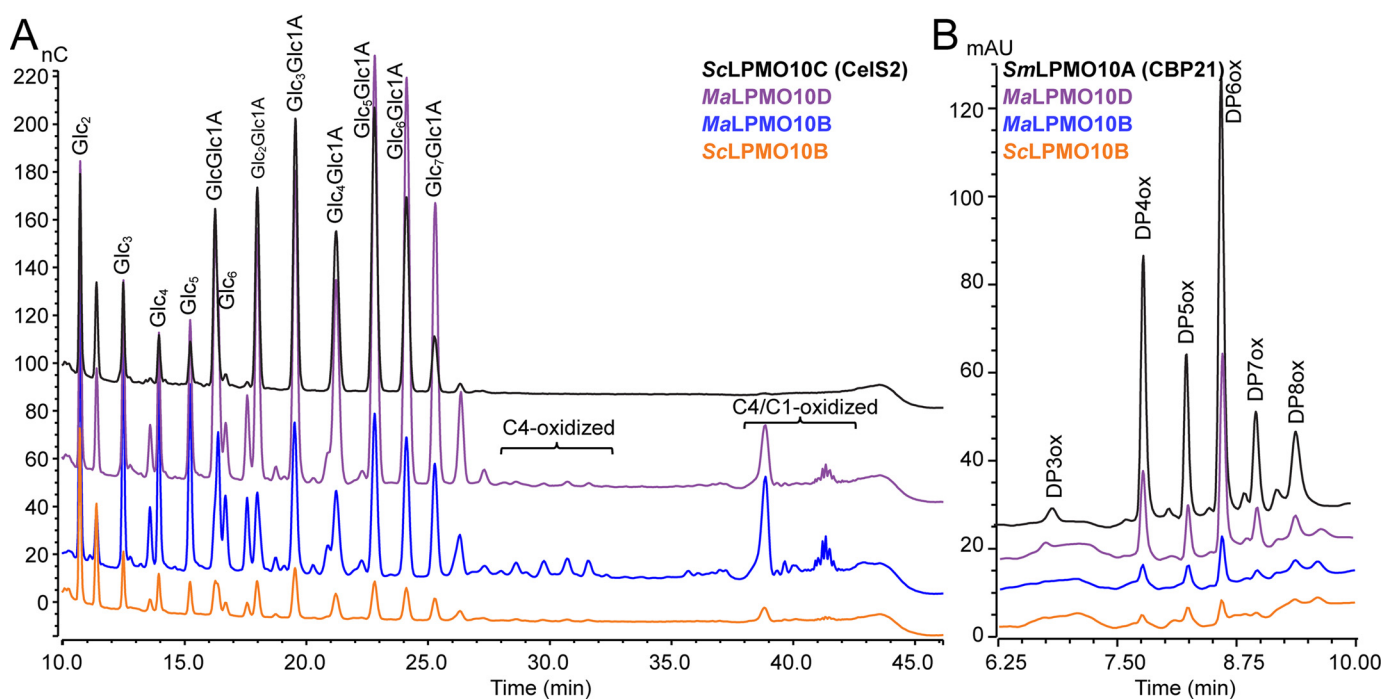


Figure 4. Chromatographic analysis of product formation by various LPMO10s. A, HPAEC-PAD detection of products released from PASC (0.2%) by ScLPMO10C (black; C1-oxidizer), MaLPMO10D (purple), MaLPMO10B (blue), and ScLPMO10B (orange). nC, nanocoulomb. B, HILIC-UV detection of oxidized products from squid pen β -chitin (1%) by SmLPMO10A (black), MaLPMO10D (purple), MaLPMO10B (blue), and ScLPMO10B (orange). All reactions were incubated for 24 h at 40 °C and 1000 rpm in 50 mM BisTris, pH 6.0, and in the presence of 1 mM ascorbic acid and 1 μ M of LPMO. No products were detected in reactions lacking ascorbic acid. For supporting mass spectrometry analysis of products, see Figs. S5 and S6. mAU, milliabsorbance unit.

Table 1

Diffraction data and refinement statistics for the MaLPMO10B^{cd} structure (PDB code 5OPF)

r.m.s.d. is root mean square deviation.

| Data collection | |
|---|-------------------------|
| Beamline | ID23–2 (ESRF, Grenoble) |
| Wavelength (Å) | 0.8726 |
| Space group | $P2_12_12_1$ |
| Unit cell dimensions | |
| <i>a</i> , <i>b</i> , <i>c</i> (Å) | 43.86, 55.09, 75.11 |
| α , β , γ | 90.0 90.0 90.0 |
| Resolution (Å) | 44.42–1.08 (1.12–1.08) |
| Unique reflections ^a | 78,485 (7545) |
| Multiplicity | 4.8 (4.0) |
| Completeness (%) | 99.8 (99.1) |
| Mean <i>I</i> / σ <i>I</i> | 11.5 (1.5) |
| <i>R</i> _{meas} ^b | 0.08 (0.85) |
| Refinement statistics | |
| <i>R</i> _{cryst} / <i>R</i> _{free} (%) ^c | 14.0/15.2 |
| r.m.s.d bond lengths (Å) | 0.006 |
| r.m.s.d angles (°) | 0.92 |
| No. of non-H atoms/ <i>B</i> -factor | |
| Protein | 1546/9.15 |
| Solvent | 325/23.01 |
| Metal | 1/7.53 |
| Ramachandran plot (%) ^d | |
| Most favored | 98.0 |
| Additionally allowed | 2.0 |
| Outliers | 0 |

^a Values in parentheses are for the highest resolution shells.

^b *R*_{meas} was defined according to Diederichs and Karplus (40).

^c $R_{\text{cryst}} = \frac{\sum_{hkl} |F_o| - \sum_{hkl} |F_c|}{\sum_{hkl} |F_o|}$, where *F*_o and *F*_c are the observed and calculated structure factor amplitudes, respectively. *R*_{free} is calculated from a randomly chosen 5.0% subset of all unique reflections not used in refinement.

^d Data were defined using MolProbity (41).

dizing LPMO10s (ScLPMO10B–Ala-148 and TjLPMO10A–Ala-142), which strengthens the observed correlation between oxidative regioselectivity and the accessibility of the axial coordination site of the copper, the latter being seemingly higher in C1/C4-oxidizers relative to strictly C1-oxidizers (Fig. 6).

Probing putative functional determinants by site-directed mutagenesis

MaLPMO10B, ScLPMO10B, and ScLPMO10C were targeted for site-directed mutagenesis, to assess the roles of the four residues identified by the CMA and to test the impact of the active-site alanine discussed above and in Ref. 25. All mutant proteins were produced in reasonable amounts and could be purified using the procedures developed for the corresponding wildtype enzymes. Table 2 lists all the mutants used in this study, including their relative activities and their oxidative regioselectivity.

In initial experiments, we addressed the observed correlation between the apparent accessibility of the solvent-exposed axial copper coordination site and oxidative regioselectivity. Ala-148 in ScLPMO10B and Ala-142 in MaLPMO10B, both C1/C4-oxidizers, are located such that they do not block access to the solvent-exposed axial copper coordination site, possibly due to a loop displacement that seems mediated by a conserved aspartate (Asp-146 in ScLPMO10B and Asp-140 in MaLPMO10B, respectively; Fig. 6, A and B). The ScLPMO10B-A148G and A148S mutants showed strongly reduced activity but still produced C4-oxidized products (see Fig. 6C, in particular the small peak corresponding to double-oxidized dimer eluting at ~40 min). The A142G mutation in ScLPMO10C reduced activity but did not endow the enzyme with C4-oxidizing ability (Fig. 6D). We also addressed the role of the conserved aspartate possibly involved in “displacing” the conserved alanine in C1/C4-oxidizers (Fig. 6, A and B). The MaLPMO10B-D140A mutant showed moderately reduced activity and essentially unchanged oxidative regioselectivity, although with a slight shift toward a

Functionality of cellulose-oxidizing LPMO10s

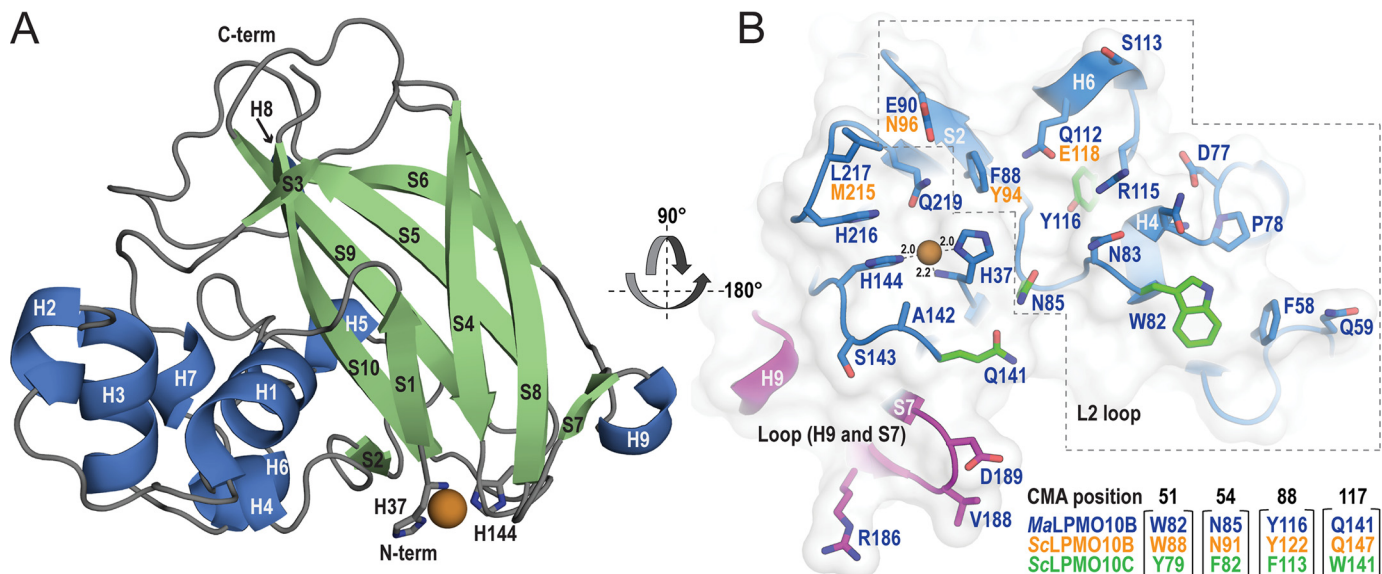


Figure 5. Three-dimensional crystal structure of *MaLPMO10B^{cd}*. *A*, secondary structure of *MaLPMO10B^{cd}* shown as cartoon with the active-site histidines (His-37 and His-144) shown as sticks and the copper ion shown as an orange sphere. The α -helices (H1–H9) are colored blue and the β -strands (S1–S10) are colored green. Helices H1–H7 occur in the region sometimes referred to as L2 loop. *B*, side chains in the substrate-binding surface of *MaLPMO10B*. Blue residue labels correspond to *MaLPMO10B* residues, and the corresponding residue is the same in *ScLPMO10B* unless otherwise stated (orange labels). The extra surface region present in *MaLPMO10B* (and in five of the other 28 C1/C4 sequences used in this study, but not in *ScLPMO10B*) is colored in magenta and includes a small helix (H9) and a short strand (S7). Side chains that were targeted for mutagenesis based on the CMA are shown as green sticks. The corresponding residues in the two *S. coelicolor* LPMOs are provided below the structure.

higher C1:C4 ratio (Fig. 6D; Table 2). All in all, these experiments do not support the suggestion, from structural comparisons, that access to the solvent-exposed axial copper coordination site is a key determinant of oxidative regioselectivity.

Table 2, Fig. 7, and Fig. S8 show the activities of a series of *MaLPMO10B* variants designed based on the outcome of the CMA and containing one to four mutations. All mutations changed the sequence of C1/C4-oxidizing *MaLPMO10B* toward the sequence of C1-oxidizing LPMO10s. The mutated variants showed C1 activities ranging from 10 to 27% of wild-type activity, whereas C4 activity was reduced to a higher extent, ranging from 1 to 15% of wildtype activity (Table 2). Thus, several of the mutants showed strongly increased C1:C4 ratios in their product mixtures, in particular mutants containing the N85F mutation (CMA position 54, Fig. 3). Quantitative analyses (Fig. 7; Table 2) showed that the N85F mutation alone changes the C1:C4 ratio from 0.9 (for the WT) to 5.9. The highest C1:C4 ratios were observed for the double mutant W82Y/N85F (10.9) and the triple mutant W82Y/N85F/Y116F (14.7). For further verification, a limited number of mutations was also made in C1/C4-oxidizing *ScLPMO10B* and C1-oxidizing *ScLPMO10C*. In accordance with the results obtained with *MaLPMO10B*, mutation of CMA positions 51 and 54 in *ScLPMO10B* (W88Y/N91F, analogous to W82Y/N85F in *MaLPMO10B*) reduced the C4 activity, in this case to undetectable levels (Fig. S9A). It should be noted that, due to the weak activity of *ScLPMO10B* and in particular of its mutants, the levels of C4-oxidized products were close to the limit of detection, meaning that it is not certain that C4 activity was eliminated completely. Introduction of reversed mutations in *ScLPMO10C* (Y79W and F82N, alone or in combination) led to a moderate reduction of activity, but it did not lead to production of C4-oxidized compounds (Table 2; Fig. S9, C and D).

Finally, the truncated *MaLPMO10B^{cd}* variant was also tested, showing reduced activity but an unchanged C1:C4 ratio (Figs. 7; Fig. S8; Table 2).

Westereng *et al.* (43) have shown chemical instability of the C4-oxidized oligosaccharides at alkaline conditions, which are used during HPAEC-PAD. The instability causes on-column decomposition and results in production of native oligosaccharides that contain one less sugar than the original C4-oxidized product. A typical chromatogram for an LPMO with C4 or mixed C1/C4 activity therefore usually shows a higher quantity of native products compared with chromatograms for a strict C1-oxidizing LPMO (see Figs. 4 and Fig. S8) (23). Thus, loss of C4-oxidizing activity in some of the mutants discussed above should also be reflected in a higher C1:native ratio, and this was indeed observed (Fig. S10).

Chitin activity of *MaLPMO10B* variants

Because all so far-characterized C1/C4-oxidizing cellulose-active LPMO10s are also active on chitinous substrates, but strict C1-oxidizing cellulose-active LPMO10s are not, the identified CMA positions may also give insight into determinants for substrate specificity. All *MaLPMO10B* variants were therefore tested for activity on chitin (Fig. S11 and Table 2). Variants with the largest reduction in C4-oxidizing activity, such as the N85F single mutant and the W82Y/N85F double mutant, showed the lowest activity on chitin. Remarkably, although the individual Y116F and Q141W mutations had relatively small effects on chitin activity, this activity was completely abolished in the W82Y/N85F/Q141W and W82Y/N85F/Y116F/Q141W mutants, both of which are active on cellulose (Fig. S8). It would thus seem that the combined substrate-binding residues targeted in this study, which were found by comparing C1- and C1/C4-oxidizing cellulose-active LPMO10s, are also essential

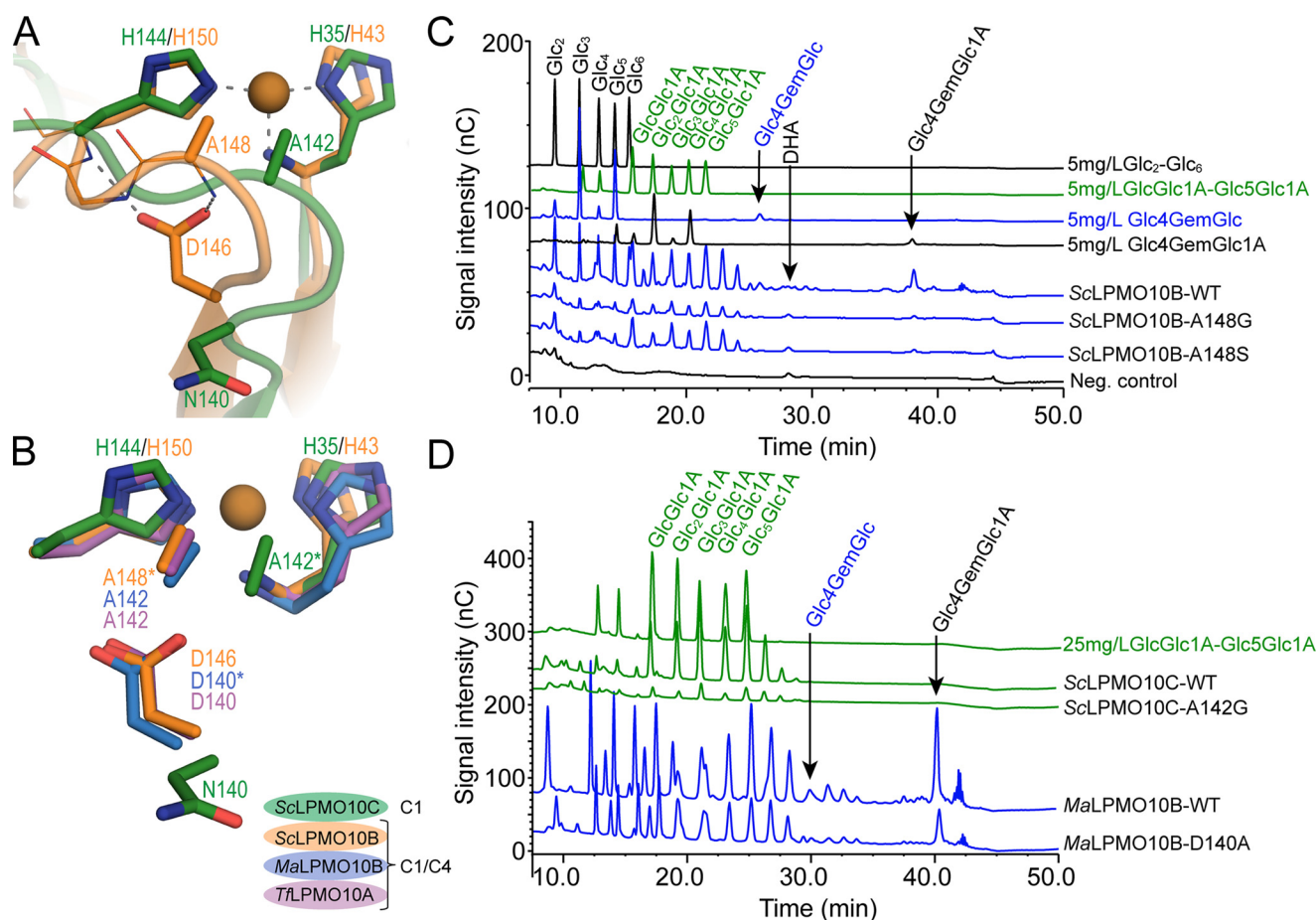


Figure 6. Structure and function of the conserved active-site alanine. A shows a superposition of the active site in ScLPMO10B (orange) and ScLPMO10C (green) and highlights how Asp-146 in ScLPMO10B and Asn-140 (ScLPMO10C) are structurally different, where Asp-146 may co-determine the position of the active-site alanine (ScLPMO10B–Ala-148). B shows how Asp-146 and Ala-148 adopt similar positions in the structures of two other C1/C4-oxidizing LPMO10s, MaLPMO10B (blue) and TrLPMO10A (purple). Mutated residues are labeled with an asterisk in B. C shows chromatograms for various standards: native cello-oligosaccharides (black), C1-oxidized cello-oligosaccharides (green), C4-oxidized dimer (blue), and C4-oxidized dimer further oxidized at the C1 position by MtCDH (black) and chromatograms for products generated by ScLPMO10B variants that reveal the effect of mutating Ala-148. The negative control shows a chromatogram of a reaction without an LPMO. D shows chromatograms that illustrate the effect of the A142G mutation in ScLPMO10C and the D140A mutation in MaLPMO10B. DHA, dehydroascorbic acid.

for activity toward chitin substrates. It is noteworthy that LPMO10s that exclusively oxidize chitin all have a threonine at CMA position 117, *i.e.* a residue that is much smaller than the Trp residue, which, when combined with a Phe at CMA position 54, abolishes chitin activity.

Stability of MaLPMO10B variants

LPMO-catalyzed reactions suffer from enzyme inactivation that is likely caused by auto-oxidation (16). To assess the stability of wildtype MaLPMO10B and a selection of mutants (WT^{cd}, W82Y, N85F, Y116F, W82Y/N85F, and W82Y/N85F/Y116F), product formation was analyzed over time (Fig. 8). Under the conditions used, the wildtype enzyme showed an increase over time for up to 8 h for both C1 and C4 products. Interestingly, several of the less active variants described above showed rates equal to or even higher than wildtype rates early in the reaction (Fig. 8B). Because these variants also show rapid enzyme inactivation, maximum product levels were reached before 2 h (Fig. 8A). Notably, if product formation had been measured after 2 h only (Fig. 8B), we would have concluded that W82Y/N85F has better activity than the wildtype, although its specificity had changed from C1/C4 to almost exclusively C1.

Careful inspection of existing data shows that deletion of carbohydrate-binding modules negatively affects the lifetime of an LPMO (25, 34, 36), and very recent data indicate that substrate binding protects the enzyme from oxidative self-inactivation (16). It is thus not surprising that truncated MaLPMO10B, which indeed binds much weaker to the substrate (Fig. S12), is among the mutants with short lifetimes (Fig. 8). To probe the early inactivation of the WT^{cd} and W82Y/N85F variant, an experiment was performed in which more substrate or more enzyme was added to the reactions at a time when product formation had ceased (Fig. S13). This experiment clearly showed that only addition of enzyme resulted in increased product formation, which implies that the unstable kinetics is due to enzyme inactivation and not to depletion of reductant-, oxygen-, or substrate-binding sites. It is noteworthy that W82Y/N85F, as well as W82Y and N85F with similar inactivation behavior, still has an intact CBM, suggesting that other factors, such as the protein configuration near the copper site, play a role in LPMO stability. The Y116F mutation is special in that it clearly reduced the initial rate but not the stability. Introduction of this mutation into the unstable but highly active double mutant W82Y/N85F reduced activity and restored stability (Fig. 8A).

Functionality of cellulose-oxidizing LPMO10s

Table 2
Overview of wild-type and mutated variants of LPMO10s and their properties

| Enzyme | Mutation(s) | Position in CMA ^a | Residue conservation ^b | Relative retained activity ^c (%) | | | Chitin activity ^d |
|-----------------------|------------------|------------------------------|--|---|------|--------------------------|------------------------------|
| | | | | C1 | C4 | Ratio C1:C4 ^c | |
| <i>Ma</i> LPMO10B | WT | | | 100 | 100 | 0.90 | + |
| | WT ^{cd} | | | 21.9 | 21.1 | 0.93 | + |
| | D140A | NP | 100% Asp | 45.9 | 33.6 | 1.23 | + |
| | W82Y | 51 | 100% Trp | 20.9 | 9.2 | 2.04 | + |
| | N85F | 54 | 82% Asn, 18% Met | 15.7 | 2.4 | 5.93 | + |
| | Y116F | 88 | 82% Tyr, 18% Asn | 15.2 | 14.7 | 0.93 | + |
| | Q141W | 117 | 71.5% Gln, 21.5% Gly 3.5% Ser, 3.5% Pro | 27.4 | 11.3 | 2.19 | + |
| | W82Y/N85F | 51/54 | | 14.5 | 1.2 | 10.94 | + |
| | N85F/Y116F | 55/88 | | 22.5 | 5.82 | | + |
| | W82Y/N85F/Y116F | 51/54/88 | | 14.2 | 0.9 | 14.69 | |
| | W82Y/N85F/Q141W | 51/54/117 | | 12.0 | 2.1 | 5.06 | – |
| W82Y/N85F/Y116F/Q141W | 51/54/88/117 | | 10.2 | 1.6 | 5.78 | – | |
| <i>Sc</i> LPMO10B | WT | | | 100 | 100 | 2.86 | |
| | A148G | NP | 96.4% Ala, 3.6% Ser | 27.1 | BDL | | |
| | A148S | NP | 96.4% Ala, 3.6% Ser | 52.4 | BDL | | |
| | W88Y/N91F | 51/54 | | 5.2 | BDL | | |
| <i>Sc</i> LPMO10C | WT | | | 100 | | | |
| | A142G | NP | 100% Ala | 16.2 | | | |
| | Y79W | 51 | 100% Tyr | 88.9 | | | |
| | F82N | 54 | 96% Phe, 4% Tyr | 57.9 | | | |
| | Y79W/F82N | 51/54 | | 41.7 | | | |
| | W141Q | 117 | 96% Trp, 4% Val | 17.6 | | | |

^a Position is in the CMA, see Fig. 3 and Tables S2–S6 for more details. NP is not part of the CMA.

^b Residue distributions are shown for the sequences used in the CMA and belonging to the same subgroup (*i.e.* C1/C4 or C1-specific cellulose-active LPMO10).

^c Data are based on quantifiable data from Fig. 7 and Fig. S9, B and D. Solubilized cello-oligosaccharides from PASC degradation were hydrolyzed by treatment with *Tf*Cel5A to generate larger amounts of fewer, quantifiable oxidized products. For *Sc*LPMO10B variants, the C4 products were below detection limits (BDL).

^d See Fig. S11 for chromatograms of chitin-active *Ma*LPMO10B variants.

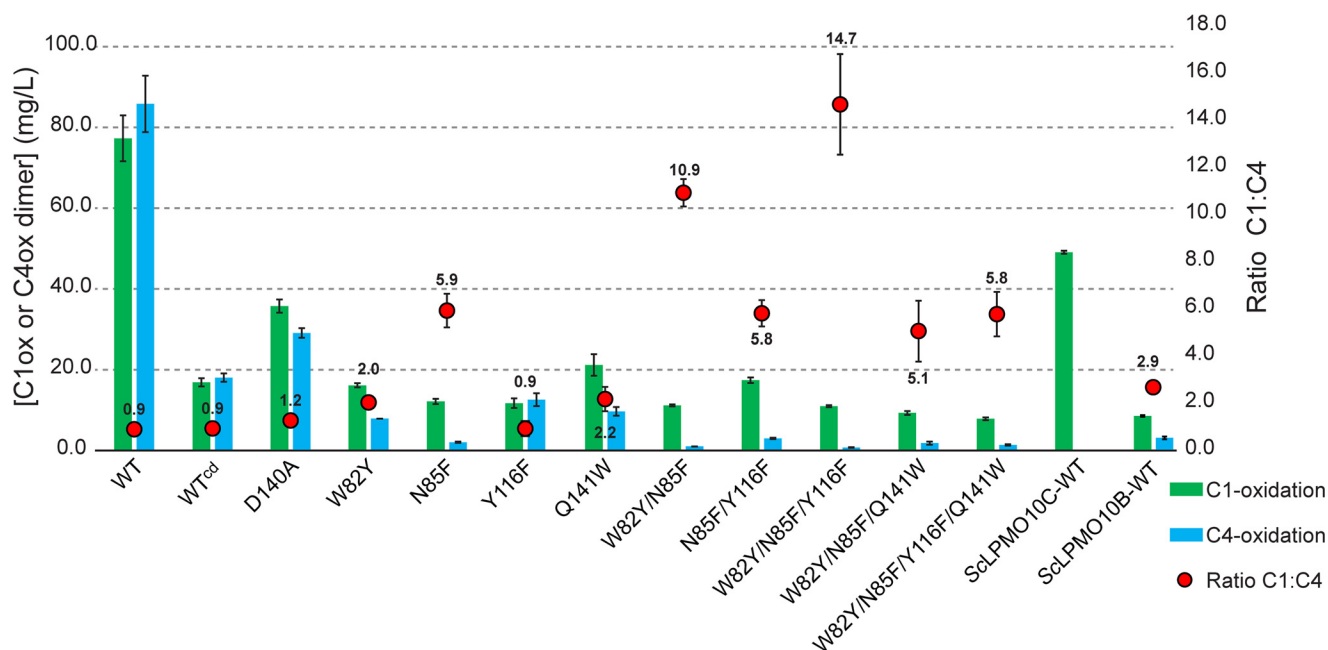


Figure 7. Quantification of C1- and C4-oxidized products generated by *Ma*LPMO10B variants. Reactions containing 0.2% PASC, 1 μ M Cu(II)-loaded LPMO, and 1 mM ascorbic acid in 50 mM BisTris buffer, pH 6.0, were incubated for 24 h at 40 °C (1000 rpm) after which solubilized cello-oligosaccharides were hydrolyzed by treatment with *Tf*Cel5A to generate larger amounts of fewer, quantifiable oxidized products. C1- and C4-oxidized dimers with known concentrations were used as standards to determine the concentration of C1-oxidized (green) and C4-oxidized (blue) products in the respective samples (see Fig. S14 for standard curves and quantification). The C1:C4 ratios are shown as red markers (secondary y axis). The error bars show \pm S.D. ($n = 3$).

H₂O₂ production and consumption

It has been shown that in the absence of substrate LPMOs produce H₂O₂ (44), whereas H₂O₂ is not detected in the presence of appropriate substrate (20). Recent data indicate that H₂O₂ generated from molecular oxygen by non-substrate-bound LPMOs may subsequently be used as co-substrate in oxidative polysaccharide cleavage by substrate-bound LPMOs

(16). Production of H₂O₂ was measured for the WT and seven of the mutants in the presence and absence of cellulose (Table 3). Insignificant H₂O₂ accumulation was observed in the reactions carried out in the presence of substrate (data not shown), but in the absence of substrate LPMO-dependent production of H₂O₂ was observed as were variations between the mutants. Most variants showed wildtype like or slightly

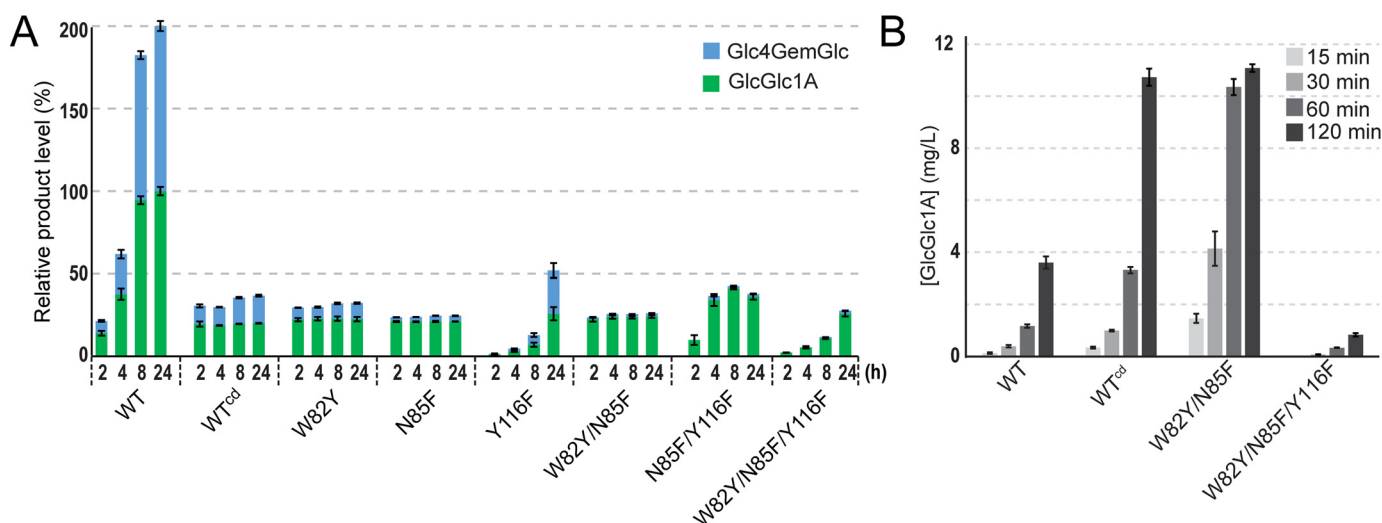


Figure 8. Production of oxidized cello-oligosaccharides over time by selected *MaLPMO10B* variants. A shows a 24-h time course and relative C1- and C4-oxidized product levels. The level of products is relative to the total quantity of products detected for the WT after 24-h reaction, set separately as 100% C1 and 100% C4. B shows the generation of C1-oxidized products during the first 2 h of the reaction. LPMOs were incubated with 0.1% PASC for up to 24 h, and solubilized cello-oligosaccharides were subsequently hydrolyzed by *TfCel5A*. C1- and C4-oxidized dimers with known concentrations were used as standards (Fig. S14) to determine the concentrations of C1-oxidized (A and B) and C4-oxidized (A) products in the respective samples. All reactions were carried out in 50 mM BisTris buffer, pH 6.0, at 40 °C with 1 μ M Cu(II)-loaded LPMO and 1 mM ascorbic acid. The error bars show \pm S.D. ($n = 3$).

Table 3

H₂O₂ production by *MaLPMO10B*-WT and variants in the absence of substrate

Reactions were carried out in a 96-well microtiter plate incubated at 40 °C. Reaction mixtures contained 1 μ M LPMO and 50 μ M ascorbic acid in 50 mM BisTris buffer, pH 6.0. Note the low concentration of ascorbic acid, which explains why levels of LPMO-independent H₂O₂ generation were low.

| Enzyme | Absolute H ₂ O ₂ production rate ^{a,b} | | H ₂ O ₂ production rate after subtraction of LPMO-independent background | | Relative H ₂ O ₂ production rate | |
|------------------|---|--------------------|--|--------------------|--|-------|
| | Average | Error ^c | Average | Error ^d | Average | Error |
| | $\mu\text{M}\cdot\text{min}^{-1}$ | | $\mu\text{M}\cdot\text{min}^{-1}$ | | % | |
| No LPMO | 0.021 | 0.002 | 0.000 | | | |
| WT | 0.364 | 0.005 | 0.344 | 0.007 | 100 | 2 |
| WT ^{cd} | 0.397 | 0.007 | 0.377 | 0.009 | 110 | 3 |
| W82Y | 0.355 | 0.014 | 0.335 | 0.016 | 97 | 5 |
| N85F | 0.236 | 0.013 | 0.215 | 0.015 | 63 | 4 |
| Y116F | 0.144 | 0.001 | 0.124 | 0.003 | 36 | 1 |
| W82Y/N85F | 0.281 | 0.003 | 0.260 | 0.005 | 76 | 2 |
| N85F/Y116F | 0.205 | 0.005 | 0.184 | 0.007 | 56 | 3 |
| W82Y/N85F/Y116F | 0.052 | 0.001 | 0.032 | 0.003 | 9 | 1 |

^a The rate was derived from the data points acquired during the 20 first min of the reaction.

^b H₂O₂ levels in similar reactions in the presence of PASC (0.195% w/v) were similar to the levels obtained in control reactions carried out in the absence of LPMO and thus are essentially negligible.

^c The error is the standard deviation derived from three replicates.

^d The error represents the sum of errors calculated for the LPMO-free reaction and the one under consideration.

reduced H₂O₂ production rates (Table 3). The Y116F-containing mutants with strongly reduced initial activity also showed the strongest reduction in H₂O₂ production. All in all, these data indicate that, likely with the exception of Y116F, the mutations did not seriously affect the ability of the LPMO to activate O₂.

The consumption of added exogenous H₂O₂ at the start of the reaction was measured for the two wildtype enzymes (WT and WT^{cd}) and the two mutants with the lowest relative H₂O₂ production rates (i.e. Y116F and the triple mutant W82Y/N85F/Y116F). The reaction mixtures contained only minute amounts (10 μ M) of ascorbic acid, which would be sufficient to carry out priming reduction for subsequent H₂O₂-driven catalysis (16), while minimizing O₂-driven catalysis, which, no matter which mechanism one assumes (12, 13), requires one molecule of ascorbic acid (or another two-electron donor) per reaction. The WT consumed all H₂O₂ during the first 15 min

(Fig. 9A) and rapid product formation occurred in that same time frame (Fig. 9B). The slow and limited further increase in product levels after 15 min for the WT corresponds well with the control reaction that lacks exogenous H₂O₂ supply. The Y116F mutant behaved in a similar manner, indicating that, although this mutation affects the enzyme's ability to activate O₂ and form H₂O₂ (Table 3), it does not affect the ability to use H₂O₂ for catalysis. The variant lacking the cellulose-binding module and the triple mutant with a reformed substrate-binding surface in the LPMO domain showed rapid enzyme inactivation (Fig. 9B) and thus incomplete enzyme-driven consumption of H₂O₂. The product levels (Fig. 9B) indicate that WT^{cd} was inactivated rapidly, long before H₂O₂ was consumed (Fig. 9A). Indeed, in this case, and in sharp contrast with WT and Y116F, the rate of H₂O₂ consumption between 15 and 120 min was similar to the background consumption measured in a control reaction with CuSO₄ (Fig. 9A).

Functionality of cellulose-oxidizing LPMO10s

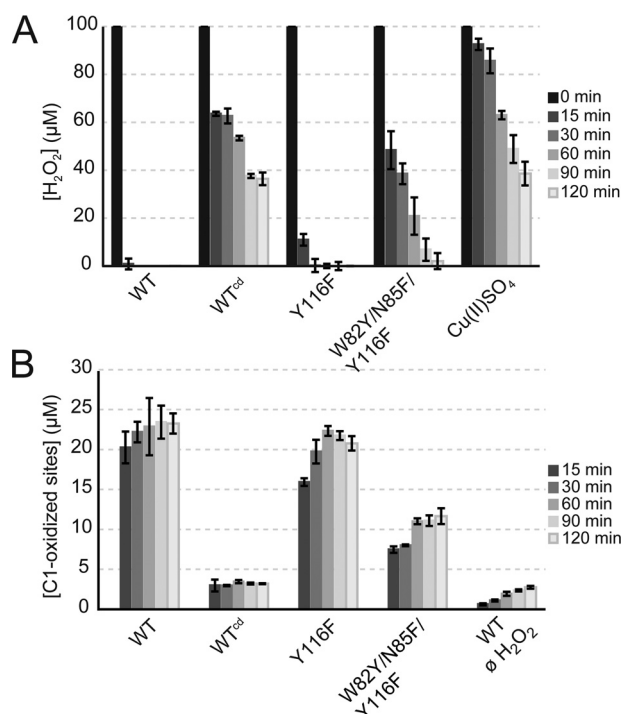


Figure 9. H₂O₂ consumption (A) and product formation (B) by selected *MaLPMO10B* variants. H₂O₂ consumption was measured in reactions containing 1 μM Cu(II)-loaded *MaLPMO10B*-WT or selected mutants with PASC (0.1%) in the presence or absence of initial exogenous H₂O₂ (100 μM). In a control reaction, LPMO-Cu(II) was replaced by 1 μM Cu(II)SO₄, and this reaction shows the background decrease in the H₂O₂ concentration. The reactions were initiated by the addition of (only) 10 μM ascorbic acid. All reactions were carried out in 50 mM sodium phosphate buffer, pH 7.0, at 40 °C. The error bars show ± S.D. (n = 3).

Discussion

The mutational effects described above provide insight into the structural determinants of the oxidative regioselectivity of LPMO10s. Somewhat unexpectedly, almost any mutation, even sets of correlated mutations, seemingly reduced LPMO activity under standard assay conditions. Measurement of progress curves for the most interesting mutants showed that, in most cases, this apparent reduction in enzyme activity is due to reduced operational enzyme stability (Fig. 8), which could be due to changes in the enzymes' ability to handle activated oxygen species, as discussed below. This leads to the conclusion that the copper sites of LPMOs and their surroundings represent a carefully balanced conformational arrangement, where multiple side chains confer specific enzyme properties (oxidative regioselectivity and substrate preferences) while maintaining sufficient operational (redox) stability. The data presented in this paper clearly show that it is imperative that any quantitative evaluation of LPMO functionality is supported by progress curves. For example, looking at Fig. 8, it is clear that if only 2-h time points had been used, the conclusions concerning catalytic activity would differ substantially from when only 24-h time points had been used.

To assess the structural determinants of oxidative regioselectivity, several mutations were made in previously described cellulose-active LPMO10s, as well as in one of two newly characterized cellulose-active LPMO10s from *M. aurantiaca*, *MaLPMO10B*. The crystal structure of the catalytic domain of CBM2-containing *MaLPMO10B* was determined. Deletion of

the CBM2 affected the operational stability of the LPMO (see below) but did not affect the C1:C4 ratio. Various mutations, in several LPMOs, that likely affect the accessibility of the solvent-exposed axial copper coordination site did affect catalytic efficiency to an extent that did not allow us to determine accurately the C1:C4 ratio. Because of low product levels, C4-oxidized products generated by the two *ScLPMO10B*-Ala-148 mutants could not be quantified, but the presence of a peak corresponding to the double-oxidized dimer (Fig. 6) revealed that these mutants were still able to oxidize the C4-carbon. Removal of Ala-142 in C1-oxidizing *ScLPMO10C* did not introduce C4 activity. Notably, the structural effects of these latter mutations, e.g. on copper coordination and substrate binding, remain unknown, and further work is needed to unravel how the conserved alanine at or near the axial copper coordination position affects LPMO functionality. It seems clear however that this alanine is not a major determinant of oxidative regioselectivity.

The CMA of LPMO10s revealed a network of correlated mutations on or close to the LPMO-substrate-binding surface. The surface location of correlated residues indicates that evolution in LPMOs is primarily restrained by substrate recognition and/or by managing catalysis at the copper site. The CMA yielded 14 positions, where residues are highly conserved within each phenotypic subgroup. Based on their position in the structure, and somewhat arbitrarily, these 14 positions were divided into three clusters, one of which, the gray cluster (Fig. 3), was subjected to mutagenesis studies. The blue cluster involves a surface loop that shows high sequence and structural variation among LPMO10s. In LPMO9s, this surface loop is conserved regardless of substrate and oxidative regioselectivity (38). Several residues in the blue cluster are known to be important for substrate binding (35) and/or to be essential for LPMO activity (45–47). Addressing this cluster by mutagenesis is challenging due to the structural variation, which complicates structural superpositions and precludes reliable mutant design. Although the mutational studies of the gray cluster did provide insights into oxidative regioselectivity and yielded variants of *MaLPMO10B* that are almost exclusively C1-oxidizing, it is also clear that the present results do not provide the complete picture. This is illustrated by the fact that the introduction of “reversed” mutations in C1-oxidizing *ScLPMO10C* did not introduce C4-oxidizing activity. Thus, future work should likely include residues in the blue cluster.

The mutational analysis focused on the gray cluster, close to the catalytic copper, comprising Trp-82 (CMA-51), Asn-85 (CMA-54), Tyr-116 (CMA-88), and Gln-141 (CMA-117) (*MaLPMO10B* numbering, with CMA numbering in parentheses) (Fig. 5B). CMA positions 51 (*MaLPMO10B*-Trp-82) and 54 (*MaLPMO10B*-Asn-85) have a modest relative correlation score of 0.83, because two different residues appear at position 54 in C1/C4-oxidizing LPMO10s, namely Asn or Met. However, the 51–54 pair is highly conserved in C1-specific cellulose-active LPMO10 sequences (Tyr-79–Phe-82 in *ScLPMO10C*). Position 54 is 100% correlated with position 88 (Tyr-116 in *MaLPMO10B*). Finally, despite its relatively low correlation score with other positions (due to different possible combinations within the C1/C4 subgroup), position 117 (*MaLPMO10B*-Gln-141) was included in the mutagenesis

strategy because it is highly conserved in C1-specific, chitin, or cellulose-active LPMO10s (Thr and Trp, respectively).

Mutation of residues in the gray cluster (Fig. 3) indeed changed the C1:C4 ratio. The most important single mutation is N85F, raising the C1:C4 ratio from approximately one to approximately five. Stronger effects were obtained upon combining mutations, which led to non-additive effects on the C1:C4 ratio, which reached 11 in the W82Y/N85F mutant and 15 in the W82Y/N85F/Y116F mutant. Data derived from standard 24-h assays (Fig. 7) gave the impression that all mutants had lost catalytic activity relative to the wildtype, but the progress curves of Fig. 8 showed that the apparent reduction in activity is due to reduced stability. The 2-h time points of Fig. 8 show that mutants N85F and W82Y/N85F are at least as active as the wildtype and have C1:C4 ratios of 8 and 20, respectively, compared with 2 for the wildtype. The Y116F mutation is an exception, as it did reduce catalytic activity while not reducing stability (Fig. 8; like for the wildtype enzyme, product formation continues over time but at a reduced level). Moreover, the Y116F mutation restored stability when added to the W82Y/N85F double mutant. The W82Y/N85F/Y116F triple mutant seems as stable as the wildtype, but it displays reduced catalytic efficiency and undetectable C4-products during the first 4 h (Fig. 8).

All in all, the mutational data for the gray cluster show that mutations in this area have a strong effect on the C1:C4 ratio, as well as on other aspects of LPMO functionality (stability and catalytic efficiency). The connections between the various mutational effects are difficult to grasp as is the considerable non-additivity of mutational effects. As recently pointed out by Danneels *et al.* (32), aromatic residues on the surface are likely to affect substrate binding and thus, possibly, the C1:C4 ratio, a notion that is corroborated by the effects of the W82Y and N85F mutations in *Ma*LPMO10B. The general picture emerging from the present and other studies is that oxidative regioselectivity is determined by the exact positioning of the substrate relative to the copper site and that variation in this positioning is the result of multiple mutations (and may vary between substrates (48)). Interestingly, structural superpositions of C1- and C1/C4-oxidizing LPMO10s with the structure of an LPMO9 in complex with cellotriose show that the N85F mutation, which is the single mutation with the largest effect on the C1:C4 ratio, is very likely to affect substrate binding (Fig. 10). Additional mutational effects, *e.g.* on stability, are likely due to changes in the ability of the copper site to generate and withstand reactive oxygen species during the reaction, which again may be related to changes in substrate positioning. This is discussed further below.

If LPMOs are provided with reductant and oxygen in the absence of substrate, they will generate H₂O₂ (20, 44), and they may become inactivated due to auto-oxidation (Fig. 11) (16). Substrate binding prevents auto-oxidation (16), and it is thus not surprising that *Ma*LPMO10B^{cd}, lacking the CBM2 and binding much less strongly to cellulose, was less stable than the wildtype. It is more surprising that several of the *Ma*LPMO10B mutants, which still contain the CBM2 and bind strongly to cellulose, also had reduced stability. This shows that high, CBM-driven affinity to the substrate is not the only determinant of productive LPMO binding. Apparently, the network of enzyme–substrate interactions near the copper site plays a role

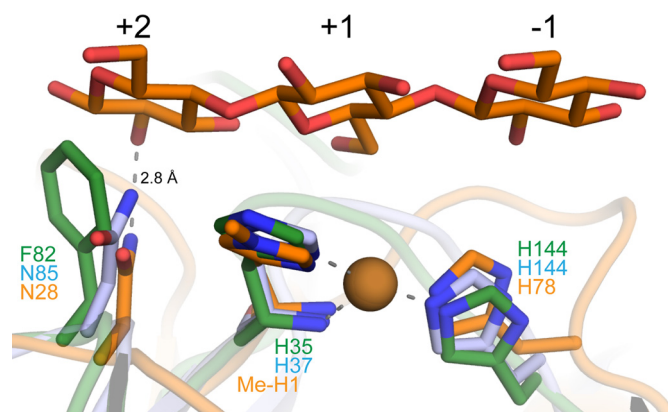


Figure 10. Structural superposition of LPMOs with different oxidative regioselectivities. The figure shows a structural superposition of C1/C4-oxidizing *Ma*LPMO10B (blue), C1-oxidizing *Sc*LPMO10C (green), and C4-oxidizing *Ls*LPMO9A bound to cellotriose (orange). Phe-82 in *Sc*LPMO10C is only 1.4 Å from the C1-carbon of the +2 sugar suggesting that, in an LPMO with Phe at this position, the substrate will be bound in a different manner compared with *Ls*LPMO9A.

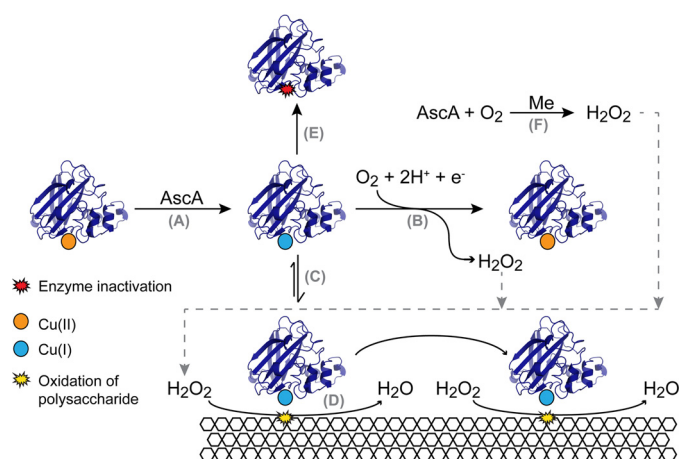


Figure 11. Schematic representation of O₂-driven polysaccharide oxidation by LPMOs assuming a catalytic mechanism that depends on H₂O₂. A shows the 1 e⁻ reduction of LPMO-Cu(II) catalyzed by ascorbic acid (or other electron donors), which may be followed by LPMO-catalyzed H₂O₂ production from O₂ (B) (44). Alternatively, the LPMO-Cu(I) may bind to substrate (C) where it uses H₂O₂ to oxidize the substrate (D); this can happen multiple times, because the LPMO stays in the Cu(I) state). H₂O₂ is not only generated by non-substrate bound LPMOs (B) but also by oxidation of ascorbic acid, which is catalyzed by trace metals (*e.g.* Fe³⁺ and Cu²⁺; abbreviated to Me) (F). Reduced LPMOs that are not bound to substrate, due to the absence of substrate or, as for some of the mutants in this study, due to impaired binding abilities, will undergo auto-oxidation leading to enzyme inactivation (E). This scheme is based on a recent study by Bissaro *et al.* (16). Other catalytic scenarios that are not dependent on the formation of H₂O₂ have recently been reviewed Refs. 12 and 13.

in channeling the redox chemistry into a productive and not self-destructive direction.

All mutants, except mutants containing Y116F, produced hydrogen peroxide in wildtype-like amounts, showing that the ability to activate molecular oxygen generally was not affected and explaining why the exception, Y116F, had a truly reduced catalytic activity. Removal of the hydroxyl group of Tyr-116, at 10.6 Å from the copper, thus diminishes the enzyme's ability to activate oxygen. It has recently been shown that LPMOs can use hydrogen peroxide rather than molecular oxygen, and there is evidence that hydrogen peroxide, which in standard reactions would be generated by the LPMO itself using molecular oxygen

Functionality of cellulose-oxidizing LPMO10s

and ascorbic acid, is the true co-substrate during polysaccharide oxidation (Fig. 11) (16). Because excess H_2O_2 damages the LPMO (16), stable enzyme kinetics can only be obtained if the rate of H_2O_2 production in a reaction does not exceed the rate of H_2O_2 consumption. The rate of H_2O_2 consumption will be affected by how well the enzyme binds to and cleaves the substrate. Experiments with added H_2O_2 showed that the Y116F consumes H_2O_2 almost as fast as the wildtype, which explains why this mutant, with decreased H_2O_2 production, shows stable kinetics. For other variants, with weakened (WT^{cd}) or changed substrate binding (all CMA mutants containing the N85F mutation), the produced wild type-like levels of H_2O_2 are apparently too high, leading to rapid enzyme inactivation. It is important to note that product formation is much faster in reactions with addition of exogenous H_2O_2 compared with reactions in which the LPMOs have to produce H_2O_2 from O_2 , thus corroborating the results of Bissaro *et al.* (16). This is especially true for the Y116F mutant that has a decreased ability to activate oxygen and, thus, produce “its own” H_2O_2 .

In a large phylogenetic study on the evolution of substrate specificity among LPMO10s, Book *et al.* (37) suggested that the ancestral form was a C1-specific chitin-oxidizing LPMO. It is conceivable that the evolution toward cellulose-active LPMOs was accompanied by loss of oxidative regioselectivity leading to mixed C1/C4-oxidizing cellulose-active LPMO10s with remaining activity toward chitin, such as *MaLPMO10B*. Further evolution toward a C1-specific cellulose-active LPMO10 could be accompanied by loss of the remaining chitin activity, as is indeed observed in Nature (C1-specific cellulose-active LPMO10s are not active on chitin) and in the mutational study presented here (mutants with increased C1:C4 ratio show reduced chitin activity). Fig. S11 shows that the N85F mutation, which is the most important single mutation leading to an increased C1:C4 ratio on cellulose, also has the largest effect on reducing chitin activity. Combination of N85F with Q141W, which alone hardly affected the C1:C4 ratio or chitin activity, abolished activity on chitin.

In conclusion, this study reveals determinants of the oxidative regioselectivity of LPMO10s, showing how a chitin- and cellulose-active C1/C4-oxidizing LPMO can be transformed to an LPMO that is only active on cellulose and that almost exclusively oxidizes C1. Importantly, the results also underpin the intricacy of these enzymes and the major challenges in experimental assessment of their functionality. It seems that many residues in the binding and catalytic surface somehow are interacting, either directly or via effects on the copper site or via their interactions with a substrate spanning the surface. As a result, mutational effects are not additive. Despite encouraging progress in recent years (6, 12, 13, 38) and in this study, it is clear that more work is needed to fully unravel how these powerful and important enzymes work.

Experimental procedures

Bioinformatics analysis

To construct the pool of sequences of C1-specific or C1/C4-oxidizing cellulose-active LPMO10s, sequences of experimentally characterized *ScLPMO10C* and *ScLPMO10B*, respec-

tively, were used as queries for protein–protein BLAST (blastp) searches against the non-redundant NCBI database, with threshold sequence identity values of 37 and 50% (based on previous phylogenetic analyses). The resulting sequences were used to construct phylogenetic trees to identify specific enzymes as sequence “boundaries,” namely *TfLPMO10B* for the C1-specific pool and *CfLPMO10C* for the C1/C4 pool. Sequences in between the sequence query and the corresponding sequence boundary in the tree were selected to constitute one pool (Table S1). Twenty six sequences were selected for the C1-specific pool and 28 sequences for the C1/C4 pool (the latter pool corresponds to clade II-B in the phylogenetic analysis of LPMO10s (37)).

Each set of sequences was then aligned using the T-Coffee Expresso on-line tool (49) using the structures of *ScLPMO10C* (PDB 4OY7) and *ScLPMO10B* (PDB 4OY6) as additional data input. The resulting MSA was employed as input to build the final phylogenetic tree (Fig. 2), using PhyML available via the on-line platform Phylogeny.fr (50),³ and to carry out the CMA. Positions in the MSA with correlated mutations were identified by applying the 3DM database’s Comulador on-line tool (33), providing a correlated position heatmap as well as a correlation network. Phylogenetic trees were visualized using the iTOL platform (51), and 3D-protein structures were visualized using the PyMOL Molecular Graphics System, Version 1.8 Schrödinger, LLC.

Cloning, expression, and purification

Codon-optimized genes encoding the *M. aurantiaca* ATCC 27029 LPMO10s *MaLPMO10B* (residues 1–366; UniProtKB D9SZQ3; signal peptide + LPMO domain + CBM2 domain) and *MaLPMO10D* (residues 36–355; UniProtKB D9T1F0; LPMO domain + CBM2 domain) were purchased from GenScript (Piscataway, NJ). Gene-specific primers (Table S7), with sequence overhangs corresponding to the pre-linearized pRSETB (Invitrogen) expression vector, were used to amplify the two *lpmo* genes generating fragments ready to be inserted into the vector using the In-Fusion[®] HD cloning kit (Clontech). *MaLPMO10B* was cloned with its native signal peptide (residues 1–36), whereas *MaLPMO10D* was cloned without its signal peptide (residues 1–35) and fused to the signal peptide of *SmLPMO10A* (residues 1–27) as described previously (46). For structural studies, a truncated version of *MaLPMO10B* was also produced (residues 1–230; called *MaLPMO10B^{cd}*) lacking the CBM2 and the linker between the two domains. Sequence-verified plasmids were transformed into One Shot[®] BL21 Star[™] (DE3) chemically competent *Escherichia coli* cells (Invitrogen) for protein expression. Cells harboring the plasmids were inoculated and grown in lysogenic broth (LB) medium supplemented with 100 μ g/ml ampicillin. Cells producing full-length LPMOs were cultivated at 30 °C for 20 h, whereas cells producing *MaLPMO10B^{cd}* were grown at 37 °C for 16 h (note that expression was driven by leakiness of the T7 promoter and that no isopropyl 1-thio- β -D-galactopyranoside (IPTG) was added).

³ Please note that the JBC is not responsible for the long-term archiving and maintenance of this site or any other third party hosted site.

Cells were harvested by centrifugation, and periplasmic extracts were generated by applying an osmotic shock method (52). The periplasmic fractions, containing the mature (*i.e.* signal peptide-free) protein, were sterilized by filtration and adjusted to 25 mM BisTris propane/HCl, pH 9.5, prior to protein purification. All *Ma*LPMO10 enzyme variants were purified by an anion-exchange chromatography method using a 5-ml HiTrap DEAE FF column (GE Healthcare) and a running buffer consisting of 25 mM Bis-Tris propane/HCl, pH 9.5. Under these conditions, most *E. coli* proteins bound to the column, whereas the full-length *Ma*LPMO10s came out pure in the flow-through. Only the truncated version of *Ma*LPMO10B, *Ma*LPMO10B^{cd}, bound to the column and was eluted by applying a linear salt gradient (0–500 mM NaCl) over 60 column volumes. LPMO-containing fractions were subsequently pooled and concentrated using Amicon ultracentrifugal filters (Millipore) with a molecular mass cutoff of 10,000 Da, and *Ma*LPMO10B^{cd} was further purified by size-exclusion chromatography using a HiLoad 16/60 Superdex 75 column operated at 1 ml/min and with a running buffer containing 50 mM Tris/HCl, pH 7.5, and 200 mM NaCl. Protein purity was verified by SDS-PAGE, and fractions containing pure protein were combined and concentrated using Amicon ultracentrifugal filters (Millipore). Two *Streptomyces coelicolor* LPMOs, *Sc*LPMO10B and *Sc*LPMO10C, were expressed and purified as described previously (25).

Before use, all enzymes were saturated with Cu(II), as described previously (53), followed by desalting using PD MidiTrap G-25 columns (GE Healthcare) equilibrated with 20 mM BisTris, pH 6.0. Protein concentrations were determined by measuring A_{280} and using the proteins' calculated molar extinction coefficients (using the ExPASy ProParam tool) to convert A_{280} to concentration (Table S8).

Site-directed mutagenesis

Plasmids encoding full-length *Ma*LPMO10B (LPMO + CBM2), *Sc*LPMO10B (only an LPMO domain), and *Sc*LPMO10C (LPMO + CBM2) were used as template for site-directed mutagenesis. The mutants listed in Table S8 were generated using the QuikChange II XL site-directed mutagenesis kit (Agilent Technologies). Mutated plasmids were verified by sequencing and thereafter used for protein expression and purification in the same way as for the wildtype enzymes (see above).

Crystallization, diffraction data collection, structure determination, and model refinement

Crystals of the catalytic LPMO10 domain of *Ma*LPMO10B (*Ma*LPMO10B^{cd}; residues 37–230) were obtained by hanging-drop vapor diffusion at room temperature by mixing equal volumes (1 μ l) of the Cu(II)-saturated LPMO solution (in 20 mM BisTris, pH 6.0) and the reservoir solution. Crystals were obtained in 0.04 M potassium phosphate monobasic and 16% w/v PEG8000 and 20% v/v glycerol at a protein concentration of 21.9 mg/ml. Crystals were retrieved from the crystallization droplets and transferred to the reservoir solution supplemented with 20% (v/v) ethylene glycol prior to flash-freezing in liquid nitrogen. X-ray diffraction images were collected at the

ID23-2 beamline at the European Synchrotron Radiation Facility (ESRF). Several crystals diffracted to ~ 1.1 Å resolution, and a selected data set was integrated, scaled, and analyzed to 1.08 Å using XDS (54), Aimless (55), and CCP4i (56). The structure was solved by molecular replacement using Phaser (57) and a polyalanine model of the *Sc*LPMO10B (PDB 4OY6 (25)). The model was rebuilt into the *Ma*LPMO10B^{cd} sequence using PHENIX (58), which was also used for the refinement. Model adjustments and map inspections were carried out using Coot (59). Riding hydrogen atoms were included for all protein residues, except for hydroxyl side chain groups of Ser, Thr, and Tyr, as well as the N-terminal amino group, which interacts with the catalytic copper ion. Atomic displacement parameters were refined for non-hydrogen atoms using eight different translation/liberation/screw (TLS) groups. The final model refined to R_{cryst} and R_{free} factors of 0.14 and 0.15, respectively.

Enzyme reactions

Standard LPMO reactions were set up with 0.1–0.2% (w/v) PASC as substrate in 50 mM BisTris buffer, pH 6.0, at 40 °C. The final LPMO concentration in the reactions was 1 μ M, and the reducing agent (L-ascorbic acid) was present in a thousand-fold surplus (1 mM), unless otherwise stated. The reactions were carried out in 2-ml Eppendorf tubes and incubated at 40 °C in an Eppendorf Comfort Thermomixer at 1000 rpm for up to 24 h. Chitin degradation reactions were set up with 1% (w/v) β -chitin (extracted from squid pen, batch 20140101, France Chitin, Orange, France) as substrate, using the same conditions as for PASC degradation. At regular intervals, samples were taken from the reactions, and the LPMO activity was stopped by immediately separating the soluble fractions from the insoluble substrate particles by filtration using a 96-well filter plate (Millipore) operated with a vacuum manifold. By separating soluble oligosaccharides from the insoluble cellulose or chitin, the activity was stopped, as the LPMOs used in this study do not oxidize soluble cello- or chito-oligosaccharides. For qualitative analysis of products generated from PASC, the filtered samples were injected onto a CarboPac PA1 column (see below) without any additional action, whereas samples for quantitative analysis were further hydrolyzed with a GH5 endoglucanase from *Thermobifida fusca* (*Tf*Cel5A (60)) yielding mixtures of glucose, cellobiose, and oxidized products with a degree of polymerization of 2 and 3 (*i.e.* GlcGlc1A, Glc₂Glc1A, Glc4GemGlc, and Glc4GemGlc₂). Standards for C1- and C4-oxidized dimers were used to quantify the products and determine the oxidative regioselectivity for wildtype and mutant LPMOs (see Fig. S14).

Cello-oligosaccharides (Glc₂–Glc₆, 95–98% purity, purchased from Sigma or Megazyme) were used as native standards. Cellobiose (98% purity, purchased from Sigma) and celotriose (95% purity, purchased from Megazyme) were used as substrates for the production of C1-oxidized dimer (cellobionic acid, GlcGlc1A) and trimer (cellotrionic acid, Glc₂Glc1A) by incubation with 1.5 μ M cellobiose dehydrogenase from *Mycobacterium thermophilum* (*Mt*CDH), as described previously for the production of lactobionic acid from lactose (11). C4-oxidized dimer (Glc4GemGlc) was produced in-house by degrading cellopentaose (Glc₅) using the C4-oxidizing LPMO9C from *Neurospora crassa* (*Nc*LPMO9C), as described previously (7). The double-ox-

Functionality of cellulose-oxidizing LPMO10s

oxidized dimer (Glc4GemGlc1A) was generated by subjecting Glc4GemGlc to treatment with 1.5 μM MtCDH.

Product analysis

Qualitative analysis of native and oxidized products in soluble fractions generated from PASC or chitin was performed by matrix-assisted laser desorption/ionization time of flight mass spectrometry (MALDI-TOF MS) (1) and/or HPAEC-PAD for cellulose samples (26) and/or hydrophilic interaction chromatography with A_{205} monitoring as described previously (53) for chitin samples. The MS samples were saturated with sodium by incubating the solubilized fraction from the LPMO reaction with 10 mM sodium chloride for 1 h on the bench. Subsequently, 1 μl samples were mixed with 2 μl of 2,5-dihydroxybenzoic acid (9 g·liter⁻¹ dissolved in 30% acetonitrile) and applied to an MTP 384 target plate ground steel TF (Bruker Daltonics) followed by drying under a stream of air. The samples were analyzed with an Ultraflex MALDI-TOF/TOF instrument (Bruker Daltonics GmbH, Bremen, Germany) equipped with a nitrogen 337-nm laser beam, using Bruker FlexAnalysis software.

HPAEC analysis of products from cellulose was conducted as described previously (26) using an ICS-5000 system from Dionex (Sunnyvale, CA) set up with a disposable electrochemical gold electrode. Five- μl samples were injected on a CarboPac PA1 (2 \times 50 mm) column operated with 0.1 M NaOH (eluent A) at a flow rate of 0.25 ml/min and a column temperature of 30 °C. Elution was achieved using a stepwise gradient with increasing amounts of eluent B (0.1 M NaOH + 1 M NaOAc), as follows: 0–10% B over 10 min; 10–30% B over 25 min; 30–100% B over 5 min; 100–0% B over 1 min; and 0% B (reconditioning) for 9 min. For quantitative analysis (*i.e.* reactions hydrolyzed by TjCel5A), a steeper gradient of acetate was used as follows: 0–10% B over 10 min; 10–14% B over 5 min; 14–30% B over 1 min; 30–100% B over 2 min; 100–0% B over 0.1; and 0% B over 10.9 min. Chromatograms were recorded using Chromeleon 7.0 software.

H₂O₂ production measurements

A reaction mixture (180 μl) containing LPMO (1 μM), horseradish peroxidase (5 units·ml⁻¹), and Amplex[®] Red (Thermo Fisher Scientific) (100 μM) in 50 mM BisTris buffer, pH 6.0, was incubated for 5 min at 40 °C in a 96-well microtiter plate in a plate reader (Multiskan[™] FC Microplate Photometer (Thermo Fisher Scientific)). The reaction was initiated by the addition of 20 μl of ascorbic acid (500 μM , *i.e.* 50 μM final concentration) in each well, and the release of resorufin was monitored at 540 nm. Resorufin is generated in stoichiometric amounts when horseradish peroxidase (HRP) catalyzes oxidation of Amplex[®] Red by H₂O₂. Control reactions in the absence of the LPMO were carried out to obtain the LPMO-independent resorufin production rate. A H₂O₂ standard curve was prepared using the same conditions (without ascorbic acid and LPMO). Reactions in which PASC (0.195% w/v) was added to the reaction mixture were also carried out, and a corresponding H₂O₂ standard curve was also made. The reactions were monitored for 90 min, and H₂O₂ production rates were derived from data points between 2 and 20 min (linear region).

H₂O₂ consumption measurements

The experiment was carried out as described by Bissaro *et al.* (16) using the method described by Kittl *et al.* (44), with modifications. Reactions containing 1 μM LPMO, 0.1% (w/v) PASC, and 10 μM ascorbic acid were incubated in 50 mM sodium phosphate, pH 7.0, at 40 °C (1000 rpm) in the presence or absence of initial exogenous H₂O₂ (100 μM). From each 400- μl reaction mixture, 60- μl samples were taken at regular intervals (15, 30, 60, 90, and 120 min) and mixed with 60 μl of 50 mM NaOAc, pH 4.5, before filtration (as described above). Thirty five μl of each filtrate was saved for oxidized product analysis (see above). To determine the H₂O₂ concentration, 50 μl of the filtrate was mixed with 50 μl of a premix containing HRP (10 units/ml), Amplex Red (200 μM) in 50 mM sodium phosphate buffer, pH 7.5. Note that the Amplex Red stock solution (10 mM) was prepared in DMSO (100%), which leads to the presence of 2% final DMSO in the 50- μl premix (*i.e.* 1% in the final 100- μl reaction). The reaction mixture (100 μl) was incubated in a 96-well microtiter plate during 10 min before recording the absorbance at 540 nm. For each set of measurements, a blank (50 mM sodium phosphate buffer, pH 7.0) and H₂O₂ standards (prepared in 50 mM sodium phosphate buffer, pH 7.0) were subjected to the same treatment.

Author contributions—Z. F. designed, performed, and analyzed the experiments and wrote the paper. B. B. designed and performed experiments and contributed to writing the paper. J. G. contributed with experimental work (site-directed mutagenesis and protein production and purification). B. D. determined the crystal structure of MaLPMO10B^{cd}. G. V.-K. contributed to supervising the work and to writing the manuscript. V. G. H. E. contributed to design and analysis of the experiments and contributed to writing the manuscript. All authors have reviewed the results and approved the final version of the manuscript.

Acknowledgment—We thank Gerdt Müller for the C4-oxidized standard.

References

1. Vaaje-Kolstad, G., Westereng, B., Horn, S. J., Liu, Z., Zhai, H., Sørli, M., and Eijsink, V. G. (2010) An oxidative enzyme boosting the enzymatic conversion of recalcitrant polysaccharides. *Science* **330**, 219–222 [CrossRef Medline](#)
2. Quinlan, R. J., Sweeney, M. D., Lo Leggio, L., Otten, H., Poulsen, J. C., Johansen, K. S., Krogh, K. B., Jørgensen, C. I., Tovborg, M., Anthonsen, A., Tryfona, T., Walter, C. P., Dupree, P., Xu, F., Davies, G. J., and Walton, P. H. (2011) Insights into the oxidative degradation of cellulose by a copper metalloenzyme that exploits biomass components. *Proc. Natl. Acad. Sci. U.S.A.* **108**, 15079–15084 [CrossRef Medline](#)
3. Phillips, C. M., Beeson, W. T., Cate, J. H., and Marletta, M. A. (2011) Cellobiose dehydrogenase and a copper-dependent polysaccharide monooxygenase potentiate cellulose degradation by *Neurospora crassa*. *ACS Chem. Biol.* **6**, 1399–1406 [CrossRef Medline](#)
4. Eibinger, M., Ganner, T., Bubner, P., Rošker, S., Kracher, D., Haltrich, D., Ludwig, R., Plank, H., and Nidetzky, B. (2014) Cellulose surface degradation by a lytic polysaccharide monooxygenase and its effect on cellulase hydrolytic efficiency. *J. Biol. Chem.* **289**, 35929–35938 [CrossRef Medline](#)
5. Vermaas, J. V., Crowley, M. F., Beckham, G. T., and Payne, C. M. (2015) Effects of lytic polysaccharide monooxygenase oxidation on cellulose structure and binding of oxidized cellulose oligomers to cellulases. *J. Phys. Chem. B* **119**, 6129–6143 [CrossRef Medline](#)

6. Harris, P. V., Xu, F., Kreel, N. E., Kang, C., and Fukuyama, S. (2014) New enzyme insights drive advances in commercial ethanol production. *Curr. Opin. Chem. Biol.* **19**, 162–170 [CrossRef Medline](#)
7. Müller, G., Várnai, A., Johansen, K. S., Eijsink, V. G., and Horn, S. J. (2015) Harnessing the potential of LPMO-containing cellulase cocktails poses new demands on processing conditions. *Biotechnol. Biofuels* **8**, 187 [CrossRef Medline](#)
8. Langston, J. A., Shaghasi, T., Abbate, E., Xu, F., Vlasenko, E., and Sweeney, M. D. (2011) Oxidoreductive cellulose depolymerization by the enzymes cellobiose dehydrogenase and glycoside hydrolase 61. *Appl. Environ. Microb.* **77**, 7007–7015 [CrossRef Medline](#)
9. Kracher, D., Scheiblbrandner, S., Felice, A. K., Breslmayr, E., Preims, M., Ludwicka, K., Haltrich, D., Eijsink, V. G., and Ludwig, R. (2016) Extracellular electron transfer systems fuel cellulose oxidative degradation. *Science* **352**, 1098–1101 [CrossRef Medline](#)
10. Garajova, S., Mathieu, Y., Beccia, M. R., Bennati-Granier, C., Biaso, F., Fanuel, M., Ropartz, D., Guigliarelli, B., Record, E., Rogniaux, H., Henrissat, B., and Berrin, J. G. (2016) Single-domain flavoenzymes trigger lytic polysaccharide monooxygenases for oxidative degradation of cellulose. *Sci. Rep.* **6**, 28276 [CrossRef Medline](#)
11. Loose, J. S., Forsberg, Z., Kracher, D., Scheiblbrandner, S., Ludwig, R., Eijsink, V. G., and Vaaje-Kolstad, G. (2016) Activation of bacterial lytic polysaccharide monooxygenases with cellobiose dehydrogenase. *Protein Sci.* **25**, 2175–2186 [CrossRef Medline](#)
12. Walton, P. H., and Davies, G. J. (2016) On the catalytic mechanisms of lytic polysaccharide monooxygenases. *Curr. Opin. Chem. Biol.* **31**, 195–207 [CrossRef Medline](#)
13. Beeson, W. T., Vu, V. V., Span, E. A., Phillips, C. M., and Marletta, M. A. (2015) Cellulose degradation by polysaccharide monooxygenases. *Annu. Rev. Biochem.* **84**, 923–946 [CrossRef Medline](#)
14. Kim, S., Ståhlberg, J., Sandgren, M., Paton, R. S., and Beckham, G. T. (2014) Quantum mechanical calculations suggest that lytic polysaccharide monooxygenases use a copper-oxy, oxygen-rebound mechanism. *Proc. Natl. Acad. Sci. U.S.A.* **111**, 149–154 [CrossRef Medline](#)
15. Kjaergaard, C. H., Qayyum, M. F., Wong, S. D., Xu, F., Hemsworth, G. R., Walton, D. J., Young, N. A., Davies, G. J., Walton, P. H., Johansen, K. S., Hodgson, K. O., Hedman, B., and Solomon, E. I. (2014) Spectroscopic and computational insight into the activation of O₂ by the mononuclear Cu center in polysaccharide monooxygenases. *Proc. Natl. Acad. Sci. U.S.A.* **111**, 8797–8802 [CrossRef Medline](#)
16. Bissaro, B., Røhr, Å. K., Müller, G., Chylenski, P., Skaugen, M., Forsberg, Z., Horn, S. J., Vaaje-Kolstad, G., and Eijsink, V. G. (2017) Oxidative cleavage of polysaccharides by monocopper enzymes depends on H₂O₂. *Nat. Chem. Biol.* **13**, 1123–1128 [CrossRef Medline](#)
17. Levasseur, A., Drula, E., Lombard, V., Coutinho, P. M., and Henrissat, B. (2013) Expansion of the enzymatic repertoire of the CAZy database to integrate auxiliary redox enzymes. *Biotechnol. Biofuels* **6**, 41 [CrossRef Medline](#)
18. Beeson, W. T., Phillips, C. M., Cate, J. H., and Marletta, M. A. (2012) Oxidative cleavage of cellulose by fungal copper-dependent polysaccharide monooxygenases. *J. Am. Chem. Soc.* **134**, 890–892 [CrossRef Medline](#)
19. Westereng, B., Ishida, T., Vaaje-Kolstad, G., Wu, M., Eijsink, V. G., Igarashi, K., Samejima, M., Ståhlberg, J., Horn, S. J., and Sandgren, M. (2011) The putative endoglucanase PcGH61D from *Phanerochaete chrysosporium* is a metal-dependent oxidative enzyme that cleaves cellulose. *PLoS One* **6**, e27807 [CrossRef Medline](#)
20. Isaksen, T., Westereng, B., Aachmann, F. L., Agger, J. W., Kracher, D., Kittl, R., Ludwig, R., Haltrich, D., Eijsink, V. G., and Horn, S. J. (2014) A C4-oxidizing lytic polysaccharide monooxygenase cleaving both cellulose and cello-oligosaccharides. *J. Biol. Chem.* **289**, 2632–2642 [CrossRef Medline](#)
21. Agger, J. W., Isaksen, T., Várnai, A., Vidal-Melgosa, S., Willats, W. G., Ludwig, R., Horn, S. J., Eijsink, V. G., and Westereng, B. (2014) Discovery of LPMO activity on hemicelluloses shows the importance of oxidative processes in plant cell wall degradation. *Proc. Natl. Acad. Sci. U.S.A.* **111**, 6287–6292 [CrossRef Medline](#)
22. Frommhagen, M., Sforza, S., Westphal, A. H., Visser, J., Hinz, S. W., Koetsier, M. J., van Berkel, W. J., Gruppen, H., and Kabel, M. A. (2015) Discovery of the combined oxidative cleavage of plant xylan and cellulose by a new fungal polysaccharide monooxygenase. *Biotechnol. Biofuels* **8**, 101 [CrossRef Medline](#)
23. Vu, V. V., Beeson, W. T., Phillips, C. M., Cate, J. H., and Marletta, M. A. (2014) Determinants of regioselective hydroxylation in the fungal polysaccharide monooxygenases. *J. Am. Chem. Soc.* **136**, 562–565 [CrossRef Medline](#)
24. Forsberg, Z., Vaaje-Kolstad, G., Westereng, B., Bunæs, A. C., Stenstrøm, Y., MacKenzie, A., Sørli, M., Horn, S. J., and Eijsink, V. G. (2011) Cleavage of cellulose by a CBM33 protein. *Protein Sci.* **20**, 1479–1483 [CrossRef Medline](#)
25. Forsberg, Z., Mackenzie, A. K., Sørli, M., Røhr, Å. K., Helland, R., Arvai, A. S., Vaaje-Kolstad, G., and Eijsink, V. G. (2014) Structural and functional characterization of a conserved pair of bacterial cellulose-oxidizing lytic polysaccharide monooxygenases. *Proc. Natl. Acad. Sci. U.S.A.* **111**, 8446–8451 [CrossRef Medline](#)
26. Westereng, B., Agger, J. W., Horn, S. J., Vaaje-Kolstad, G., Aachmann, F. L., Stenstrom, Y. H., and Eijsink, V. G. (2013) Efficient separation of oxidized cello-oligosaccharides generated by cellulose-degrading lytic polysaccharide monooxygenases. *J. Chromatogr. A* **1271**, 144–152 [CrossRef Medline](#)
27. Aachmann, F. L., Sørli, M., Skjåk-Bræk, G., Eijsink, V. G., and Vaaje-Kolstad, G. (2012) NMR structure of a lytic polysaccharide monooxygenase provides insight into copper binding, protein dynamics, and substrate interactions. *Proc. Natl. Acad. Sci. U.S.A.* **109**, 18779–18784 [CrossRef Medline](#)
28. Frandsen, K. E., Simmons, T. J., Dupree, P., Poulsen, J. C., Hemsworth, G. R., Ciano, L., Johnston, E. M., Tovborg, M., Johansen, K. S., von Freiesleben, P., Marmuse, L., Fort, S., Cottaz, S., Driguez, H., Henrissat, B., et al. (2016) The molecular basis of polysaccharide cleavage by lytic polysaccharide monooxygenases. *Nat. Chem. Biol.* **12**, 298–303 [CrossRef Medline](#)
29. Hemsworth, G. R., Taylor, E. J., Kim, R. Q., Gregory, R. C., Lewis, S. J., Turkenburg, J. P., Parkin, A., Davies, G. J., and Walton, P. H. (2013) The copper active site of CBM33 polysaccharide oxygenases. *J. Am. Chem. Soc.* **135**, 6069–6077 [CrossRef Medline](#)
30. Courtade, G., Wimmer, R., Røhr, Å. K., Preims, M., Felice, A. K., Dimarogona, M., Vaaje-Kolstad, G., Sørli, M., Sandgren, M., Ludwig, R., Eijsink, V. G., and Aachmann, F. L. (2016) Interactions of a fungal lytic polysaccharide monooxygenase with β-glucan substrates and cellobiose dehydrogenase. *Proc. Natl. Acad. Sci. U.S.A.* **113**, 5922–5927 [CrossRef Medline](#)
31. Borisova, A. S., Isaksen, T., Dimarogona, M., Kognole, A. A., Mathiesen, G., Várnai, A., Røhr, Å. K., Payne, C. M., Sørli, M., Sandgren, M., and Eijsink, V. G. (2015) Structural and functional characterization of a lytic polysaccharide monooxygenase with broad substrate specificity. *J. Biol. Chem.* **290**, 22955–22969 [CrossRef Medline](#)
32. Danneels, B., Tanghe, M., Joosten, H. J., Gundinger, T., Spadiut, O., Stals, I., and Desmet, T. (2017) A quantitative indicator diagram for lytic polysaccharide monooxygenases reveals the role of aromatic surface residues in HfLPMO9A regioselectivity. *PLoS One* **12**, e0178446 [CrossRef Medline](#)
33. Kuipers, R. K., Joosten, H. J., Verwiel, E., Paans, S., Akerboom, J., van der Oost, J., Leferink, N. G., van Berkel, W. J., Vriend, G., and Schaap, P. J. (2009) Correlated mutation analyses on super-family alignments reveal functionally important residues. *Proteins* **76**, 608–616 [CrossRef Medline](#)
34. Crouch, L. I., Labourel, A., Walton, P. H., Davies, G. J., and Gilbert, H. J. (2016) The contribution of non-catalytic carbohydrate binding modules to the activity of lytic polysaccharide monooxygenases. *J. Biol. Chem.* **291**, 7439–7449 [CrossRef Medline](#)
35. Vaaje-Kolstad, G., Houston, D. R., Riemen, A. H., Eijsink, V. G., and van Aalten, D. M. (2005) Crystal structure and binding properties of the *Serratia marcescens* chitin-binding protein CBP21. *J. Biol. Chem.* **280**, 11313–11319 [CrossRef Medline](#)
36. Forsberg, Z., Nelson, C. E., Dalhus, B., Mekasha, S., Loose, J. S., Crouch, L. I., Røhr, Å. K., Gardner, J. G., Eijsink, V. G., and Vaaje-Kolstad, G. (2016) Structural and functional analysis of a lytic polysaccharide monooxygenase important for efficient utilization of chitin in *Cellvibrio japonicus*. *J. Biol. Chem.* **291**, 7300–7312 [CrossRef Medline](#)
37. Book, A. J., Yennamalli, R. M., Takasuka, T. E., Currie, C. R., Phillips, G. N., Jr., and Fox, B. G. (2014) Evolution of substrate specificity in bacterial

- AA10 lytic polysaccharide monoxygenases. *Biotechnol. Biofuels* **7**, 109 [CrossRef Medline](#)
38. Vaaje-Kolstad, G., Forsberg, Z., Loose, J. S., Bissaro, B., and Eijsink, V. G. (2017) Structural diversity of lytic polysaccharide monoxygenases. *Curr. Opin. Struct. Biol.* **44**, 67–76 [CrossRef Medline](#)
39. Wu, M., Beckham, G. T., Larsson, A. M., Ishida, T., Kim, S., Payne, C. M., Himmel, M. E., Crowley, M. F., Horn, S. J., Westereng, B., Igarashi, K., Samejima, M., Ståhlberg, J., Eijsink, V. G., and Sandgren, M. (2013) Crystal structure and computational characterization of the lytic polysaccharide monoxygenase GH61D from the Basidiomycota fungus *Phanerochaete chrysosporium*. *J. Biol. Chem.* **288**, 12828–12839 [CrossRef Medline](#)
40. Diederichs, K., and Karplus, P. A. (1997) Improved R-factors for diffraction data analysis in macromolecular crystallography. *Nat. Struct. Biol.* **4**, 269–275 [CrossRef Medline](#)
41. Chen, V. B., Arendall, W. B., 3rd., Headd, J. J., Keedy, D. A., Immormino, R. M., Kapral, G. J., Murray, L. W., Richardson, J. S., and Richardson, D. C. (2010) MolProbity: all-atom structure validation for macromolecular crystallography. *Acta Crystallogr. D Biol. Crystallogr.* **66**, 12–21 [CrossRef Medline](#)
42. Gudmundsson, M., Kim, S., Wu, M., Ishida, T., Momeni, M. H., Vaaje-Kolstad, G., Lundberg, D., Royant, A., Ståhlberg, J., Eijsink, V. G., Beckham, G. T., and Sandgren, M. (2014) Structural and electronic snapshots during the transition from a Cu(II) to Cu(I) metal center of a lytic polysaccharide monoxygenase by X-ray photoreduction. *J. Biol. Chem.* **289**, 18782–18792 [CrossRef Medline](#)
43. Westereng, B., Arntzen, M. Ø., Aachmann, F. L., Várnai, A., Eijsink, V. G., and Agger, J. W. (2016) Simultaneous analysis of C1 and C4 oxidized oligosaccharides, the products of lytic polysaccharide monoxygenases acting on cellulose. *J. Chromatogr. A* **1445**, 46–54 [CrossRef Medline](#)
44. Kittl, R., Kracher, D., Burgstaller, D., Haltrich, D., and Ludwig, R. (2012) Production of four *Neurospora crassa* lytic polysaccharide monoxygenases in *Pichia pastoris* monitored by a fluorimetric assay. *Biotechnol. Biofuels* **5**, 79 [CrossRef Medline](#)
45. Harris, P. V., Welner, D., McFarland, K. C., Re, E., Navarro Poulsen, J. C., Brown, K., Salbo, R., Ding, H., Vlasenko, E., Merino, S., Xu, F., Cherry, J., Larsen, S., and Lo Leggio, L. (2010) Stimulation of lignocellulosic biomass hydrolysis by proteins of glycoside hydrolase family 61: structure and function of a large, enigmatic family. *Biochemistry* **49**, 3305–3316 [CrossRef Medline](#)
46. Forsberg, Z., Røhr, A. K., Mekasha, S., Andersson, K. K., Eijsink, V. G., Vaaje-Kolstad, G., and Sørlie, M. (2014) Comparative study of two chitin-active and two cellulose-active AA10-type lytic polysaccharide monoxygenases. *Biochemistry* **53**, 1647–1656 [CrossRef Medline](#)
47. Span, E. A., Suess, D. L., Deller, M. C., Britt, R. D., and Marletta, M. A. (2017) The role of the secondary coordination sphere in a fungal polysaccharide monoxygenase. *ACS Chem. Biol.* **12**, 1095–1103 [CrossRef Medline](#)
48. Simmons, T. J., Frandsen, K. E. H., Ciano, L., Tryfona, T., Lenfant, N., Poulsen, J. C., Wilson, L. F. L., Tandrup, T., Tovborg, M., Schnorr, K., Johansen, K. S., Henrissat, B., Walton, P. H., Lo Leggio, L., and Dupree, P. (2017) Structural and electronic determinants of lytic polysaccharide monoxygenase reactivity on polysaccharide substrates. *Nat. Commun.* **8**, 1064 [CrossRef Medline](#)
49. Armougom, F., Moretti, S., Poirot, O., Audic, S., Dumas, P., Schaeli, B., Keduas, V., and Notredame, C. (2006) Espresso: automatic incorporation of structural information in multiple sequence alignments using 3D-Coffee. *Nucleic Acids Res.* **34**, W604–W608 [CrossRef Medline](#)
50. Dereeper, A., Guignon, V., Blanc, G., Audic, S., Buffet, S., Chevenet, F., Dufayard, J. F., Guindon, S., Lefort, V., Lescot, M., Claverie, J. M., and Gascuel, O. (2008) Phylogeny.fr: robust phylogenetic analysis for the non-specialist. *Nucleic Acids Res.* **36**, W465–W469 [CrossRef Medline](#)
51. Letunic, I., and Bork, P. (2011) Interactive Tree Of Life v2: online annotation and display of phylogenetic trees made easy. *Nucleic Acids Res.* **39**, W475–W478 [CrossRef Medline](#)
52. Manoil, C., and Beckwith, J. (1986) A genetic approach to analyzing membrane protein topology. *Science* **233**, 1403–1408 [CrossRef Medline](#)
53. Loose, J. S., Forsberg, Z., Fraaije, M. W., Eijsink, V. G., and Vaaje-Kolstad, G. (2014) A rapid quantitative activity assay shows that the *Vibrio cholerae* colonization factor GbpA is an active lytic polysaccharide monoxygenase. *FEBS Lett.* **588**, 3435–3440 [CrossRef Medline](#)
54. Kabsch, W. (2010) XDS. *Acta Crystallogr. D Biol. Crystallogr.* **66**, 12 [CrossRef](#)–132 [Medline](#)
55. Evans, P. R., and Murshudov, G. N. (2013) How good are my data and what is the resolution? *Acta Crystallogr. D Biol. Crystallogr.* **69**, 1204–1214 [CrossRef Medline](#)
56. Winn, M. D., Ballard, C. C., Cowtan, K. D., Dodson, E. J., Emsley, P., Evans, P. R., Keegan, R. M., Krissinel, E. B., Leslie, A. G., McCoy, A., McNicholas, S. J., Murshudov, G. N., Pannu, N. S., Potterton, E. A., Powell, H. R., et al. (2011) Overview of the CCP4 suite and current developments. *Acta Crystallogr. D Biol. Crystallogr.* **67**, 235–242 [CrossRef Medline](#)
57. McCoy, A. J., Grosse-Kunstleve, R. W., Adams, P. D., Winn, M. D., Storoni, L. C., and Read, R. J. (2007) Phaser crystallographic software. *J. Appl. Crystallogr.* **40**, 658–674 [CrossRef Medline](#)
58. Adams, P. D., Afonine, P. V., Bunkóczi, G., Chen, V. B., Davis, I. W., Echols, N., Headd, J. J., Hung, L. W., Kapral, G. J., Grosse-Kunstleve, R. W., McCoy, A. J., Moriarty, N. W., Oeffner, R., Read, R. J., Richardson, D. C., et al. (2010) PHENIX: a comprehensive Python-based system for macromolecular structure solution. *Acta Crystallogr. D Biol. Crystallogr.* **66**, 213–221 [CrossRef Medline](#)
59. Emsley, P., Lohkamp, B., Scott, W. G., and Cowtan, K. (2010) Features and development of Coot. *Acta Crystallogr. D Biol. Crystallogr.* **66**, 486–501 [CrossRef Medline](#)
60. Irwin, D. C., Spezio, M., Walker, L. P., and Wilson, D. B. (1993) Activity studies of eight purified cellulases: Specificity, synergism, and binding domain effects. *Biotechnol. Bioeng.* **42**, 1002–1013 [CrossRef Medline](#)

Structural determinants of bacterial lytic polysaccharide monooxygenase functionality

Zarah Forsberg, Bastien Bissaro, Jonathan Gullesen, Bjørn Dalhus, Gustav Vaaje-Kolstad and Vincent G. H. Eijsink

J. Biol. Chem. 2018, 293:1397-1412.

doi: 10.1074/jbc.M117.817130 originally published online December 8, 2017

Access the most updated version of this article at doi: [10.1074/jbc.M117.817130](https://doi.org/10.1074/jbc.M117.817130)

Alerts:

- [When this article is cited](#)
- [When a correction for this article is posted](#)

[Click here](#) to choose from all of JBC's e-mail alerts

This article cites 60 references, 19 of which can be accessed free at <http://www.jbc.org/content/293/4/1397.full.html#ref-list-1>